Evaluation of local similarity theory in the wintertime nocturnal boundary layer over heterogeneous surface

Babić, Karmen; Rotach, Mathias W.; Bencetić Klaić, Zvjezdana

http://dx.doi.org/10.1016/j.agrformet.2016.07.002

Evaluation of Local Similarity Theory in the Wintertime Nocturnal Boundary Layer over Heterogeneous Surface

Karmen Babić[1], Mathias W. Rotach[2] and Zvjezdana B. Klaić[1]

[1] *Department of Geophysics, Faculty of Science, University of Zagreb, Zagreb, Croatia.*

[2] *Institute of Atmospheric and Cryospheric Sciences, University of Innsbruck, Innsbruck, Austria.*

Abstract: The local scaling approach was examined based on the multi-level measurements of atmospheric turbulence in the wintertime (December 2008– February 2009) stable atmospheric boundary layer (SBL) established over a heterogeneous surface influenced by mixed agricultural, industrial and forest surfaces. The heterogeneity of the surface was characterized by spatial variability of both roughness and topography. Nieuwstadt's local scaling approach was found to be suitable for the representation of all three wind velocity components. For neutral conditions, values of all three non-dimensional velocity variances were found to be smaller at the lowest measurement level and larger at higher levels in comparison to classical values found over flat terrain. Influence of surface heterogeneity was reflected in the ratio of observed dimensionless standard deviation of the vertical wind component and corresponding values of commonly used similarity formulas for flat and homogeneous terrain showing considerable variation with wind direction. The roughness sublayer influenced wind variances, and consequently the turbulent kinetic energy and correlation coefficients at the lowest measurement level, but not the wind shear profile. The observations support the classical linear expressions for the dimensionless wind shear (ϕ_m) even over inhomogeneous terrain after removing data points associated with the flux Richardson number (*Rf*) greater than 0.25. Leveling-off of ϕ_m at higher stabilities was found to be a result of the large number of data characterized by small-scale turbulence (*Rf* > 0.25). Deviations from linear expressions were shown to be mainly due to this small-scale turbulence rather than due to the surface heterogeneities, supporting the universality of this relationship. Additionally, the flux-gradient dependence on stability did not show different behavior for different wind regimes, indicating that the stability parameter is sufficient predictor for flux-gradient relationship. Data followed local *z*-less scaling for ϕ_m when the prerequisite *Rf* ≤0.25 was imposed.

Key words: Stable boundary layer, Local scaling, Forest canopy, Roughness sublayer, Turbulent kinetic energy

Corresponding author at: Department of Geophysics, Faculty of Science, University of Zagreb, Horvatovac 95, 10000 Zagreb, Croatia. Tel: +385 1 460 59 26.

E-mail address: babick@gfz.hr (K. Babić)

1. Introduction

Stable atmospheric boundary layers (SBLs) are influenced by many independent forcings, such as, (sub)mesoscale motions, which act on a variety of time and space scales, net radiative cooling, temperature advection, surface roughness and surface heterogeneity (Mahrt, 2014) enhancing the complexities and posing challenges in the study of the SBL. The fate of pollutants in the boundary layer is strongly affected by turbulence which is extremely complicated in complex terrain and over heterogeneous surfaces. Moreover, due to weak turbulence the SBL is generally favorable for the establishment of air pollution episodes. Atmospheric dispersion models, used for air quality studies, as well as high-resolution regional models use similarity scaling to model flow characteristics and dispersion in such environments.

Monin-Obukhov similarity theory (MOST) (Monin and Obukhov, 1954; Obukhov, 1946) relates surface turbulent fluxes to vertical gradients, variances and scaling parameters. The assumptions underlying MOST include stationary atmospheric turbulence, surface homogeneity and the existence of an inertial sublayer (that is, surface layer, SL). Relations between these parameters (Businger et al., 1971; Dyer, 1974) are based on several experimental campaigns conducted over horizontally homogeneous and flat (HHF) surfaces (Kaimal and Wyngaard, 1990), where the original assumptions are considered to be met. Originally, MOST was based on surface fluxes, which were assumed to be constant with height, and equal to surface values within the SL (also referred to as constant-flux layer). In the unstable boundary layer, MOST has been extensively studied and proven useful in relating turbulent fluxes to profiles (Businger et al., 1971; Dyer, 1974; Wyngaard and Coté, 1972). However, the applicability of MOST in the stable SL (e.g. Cheng et al., 2005; Trini Castelli and Falabino, 2013) and over complex (Babić et al., 2016; Nadeau et al., 2013; Stiperski and Rotach, 2016) and heterogeneous surfaces is still an open issue due to many difficulties when applying traditional scaling rules since MOST assumptions may not be fulfilled. Nieuwstadt (1984) extended Monin-Obukhov similarity in terms of a local scaling approach. This regime represents the extension of MOST above the SL. Accordingly, all MOST variables are based on the local fluxes at a certain height z instead of using surface values. As MOST should be valid over flat and homogeneous terrain, studies of the SBL in terms of surface layer and local scaling approaches were made over areas characterized by long and uniform fetch conditions, such as, Greenland, Arctic pack ice and Antarctica (Forrer and Rotach, 1997; Grachev et al., 2013, 2007; Sanz Rodrigo and Anderson, 2013). Forrer and Rotach (1997) concluded that local scaling is superior over surface layer scaling. This was mainly due to the fact that surface layer over an ice sheet, with continuously stable stratification, can be very shallow (< 10 m). Moreover, for cases of strong stability, non-dimensional similarity functions for momentum and heat were in agreement with the results obtained from the local scaling approach. Grachev et al. (2013) examined limits of applicability of local similarity theory in the SBL by revisiting the concept of a critical Richardson number.

Even modest surface heterogeneity can significantly influence the nocturnal boundary layer (NBL) and lead to turbulence at higher Richardson numbers in comparison with homogeneous surfaces (Derbyshire, 1995). Since the earth's solid surfaces are mainly heterogeneous (at least to a certain degree), the interest in flow and turbulence characteristics over complex surfaces has increased in recent decades. Moreover, a proper representation of turbulence is particularly important for parameterization of surface-atmosphere exchange processes in atmospheric models (e.g., dispersion, numerical weather prediction or regional models). The turbulence characteristics have been studied through direct measurements for different complex surfaces including, complex forest sites (e.g. Dellwik and Jensen, 2005; Nakamura and Mahrt, 2001; Rannik, 1998), agricultural fields, such as, apple orchard (e.g. de Franceschi et al., 2009) or rice plantation (e.g. Moraes et al., 2005), metre-scale inhomogeneity (Andreas et al., 1998a), urban areas (e.g. Fortuniak et al., 2013; Wood et al., 2010), and complex mountainous terrains (e.g. Rotach et al., 2008), addressing to both valley floors (e.g. de Franceschi et al., 2009; Moraes et al., 2005; Rotach et al., 2004) and steep slopes (Nadeau et al., 2013; Stiperski and Rotach, 2016). However, most of these studies are associated with flows over homogeneous surfaces. In recent years much effort has been put into simulations of turbulent fluxes over relatively heterogeneous surfaces using large-eddy simulations (LES, e.g. Calaf et al., 2014). Bou-Zeid et al. (2007) used LES over surfaces with varying roughness lengths to assess the parameterization for the equivalent surface roughness and the blending height in the neutral boundary layer at regional scales. Large eddy simulations of surface heterogeneity effects on regional scale fluxes and turbulent mixing in the stably stratified boundary layers were studied by Miller and Stoll, 2013; Mironov and Sullivan, 2010; Stoll and Porté-Agel, 2008.

The vertical structure of the atmospheric boundary layer is traditionally partitioned into a SL, an outer layer and the entrainment zone (e.g. Mahrt, 2000). The SL, in turn, is subdivided into a canopy layer (CL), a roughness sublayer (RSL) and inertial sublayer. Over surfaces with small roughness elements the latter, which corresponds to the true equilibrium layer, is often identified with SL. These concepts are less applicable over heterogeneous surfaces but for the SBL they provide, nevertheless, a useful starting point.

Above very rough surfaces, such as forests or agricultural crops, the RSL has a non-negligible extension. Due to the influence of individual roughness elements on the flow within the RSL (e.g. Finnigan, 2000; Katul et al., 1999), MOST is not widely accepted. The existence of large-scale coherent turbulent structures within the RSL, which are generated at the canopy top through an inviscid instability mechanism (Raupach et al., 1996), is thought to be a reason for the failure of standard flux-gradient relationships (Harman and Finnigan, 2010).

In the scientific community substantial effort was made to address MOST in different conditions. Most of the observational studies are based on measurements from a single tower, and sometimes they result in inconsistent conclusions on the applicability of similarity theory. These inconsistencies are mostly found for studies of MOST in complex terrain (e.g. de Franceschi et al., 2009; Kral et al., 2014; Martins et al., 2009; Nadeau et al., 2013) or for small scale turbulence for which *z*-less scaling regime should apply (e.g. Basu et al., 2006; Cheng and Brutsaert, 2005; Forrer and Rotach, 1997; Grachev et al., 2013; Pahlow et al., 2001). The main objective of the present paper is to examine the applicability of local similarity scaling over a heterogeneous terrain influenced by a mixture of forest, agricultural and industrial surfaces, based on multi-level turbulence observations in the wintertime SBL. Many of the above mentioned studies in complex terrain are mainly characterized by homogeneous surface roughness, while studies over heterogeneous and patchy vegetation are still scarce in the literature. Additionally, this paper relates to the approach of Grachev et al. (2013), who investigated the limits of applicability of local similarity theory in the SBL over idealized homogeneous surface of the Arctic pack ice. In the present work we use their approach to distinguish between Kolmogorov and non-Kolmogorov turbulence, and consequently, to investigate whether classical linear flux-gradient relationships can be applied for non-homogeneous surfaces. The paper is organized as follows: in Section 2, we give a brief overview of the local scaling approach. In Section 3, we describe the measurement site and measurements and we provide a description of post processing procedures. Section 4 contains our results for scaled standard deviations of wind components, turbulent kinetic energy, turbulent exchange coefficients and non-dimensional wind profile. A summary and conclusions are given in Section 5.

2. Local scaling

Holtslag and Nieuwstadt (1986) presented an overview of scaling regimes for the SBL. Each of the scaling regimes is characterized by different scaling parameters. The turbulence in the SL can be described by MOST with surfaces fluxes of heat and momentum and the height z as scaling parameters. In this layer the relevant scaling parameter is the Obukhov length L (Obukhov, 1946), given by

$$L = -\frac{u_*^3}{k\frac{g}{\overline{\theta_v}}(\overline{w'\theta'_v})_s} \tag{1}$$

where $u_* = (\overline{u'w'_s}^2 + \overline{v'w'_s}^2)^{1/4}$ is the surface friction velocity, $(\overline{w'\theta'_v})_s$ is the surface kinematic heat flux, $\overline{\theta_v}$ is the virtual potential temperature, g is the acceleration due to the gravity, k=0.4 is the von Kármán constant. Overbars and primes denote time averaging and fluctuating quantities, respectively.

Above the SL, the local scaling regime applies, a regime proposed by Nieuwstadt (1984). According to Nieuwstad's local similarity approach, properly scaled turbulence statistics should solely be a function of the local stability parameter $\varsigma_l = (z-d)/\Lambda$, where z is the measurement height, d is zero-plane displacement height and Λ is the local Obukhov length. Even if Nieuwstadt (1984) was not referring to rough surfaces, we have introduced d as we will be concerned with data from a site where the canopy height is non-negligible. In the local scaling framework, the local Obukhov length is based on the local fluxes at height z and varies with height

$$\Lambda = -\frac{u_{*l}^3}{k\frac{g}{\overline{\theta_v}}\overline{w'\theta'_v}} \tag{2}$$

where u_{*l} indicates local friction velocity and $\overline{w'\theta'_v}$ is the local heat flux. Holtslag and Nieuwstadt (1986, their Fig. 2) showed that in the part of the SBL which encompasses a layer between 10 and 50 % of the total BL height at neutral stability and is exponentially decreasing with increasing stability, $\Lambda \approx L$. This indicates that the use of *(z-d)/Λ*, which is required by local scaling, is almost equivalent to the SL scaling parameter *(z-d)/L*. Therefore, the local scaling approach can be viewed as an extension of MOST for the entire SBL.

For large values of z/Λ ($z/\Lambda \rightarrow \infty$), the dependence on z disappears because stable stratification restricts vertical motion causing turbulence scales to be very small. Wyngaard and Coté (1972) named this limit "local z-less stratification" (height-independent). Based on the observations from a tall tower (Cabauw), Nieuwstadt (1984) found this limit to be for $\zeta_l > 1$.

Evaluation of second-order moments, especially of wind velocity standard deviations provides a good understanding of turbulence statistics. According to similarity theory, dimensionless quantities should be universal functions of the non-dimensional stability parameter. In the local scaling framework, standard deviations of wind speed components σ_i, where $i = (u, v, w)$ denotes longitudinal, lateral and vertical velocity components, respectively, are scaled as

$$\phi_i = \frac{\sigma_i}{u_{*l}} \tag{3}$$

where ϕ_i represents a set of universal similarity functions, different for each velocity component. In the literature different formulations of the ϕ_i functions can be found. de Franceschi et al. (2009) presented a comprehensive review of various formulations of ϕ_i functions suggested by different studies and for different stabilities. A generally accepted form of the flux-variance similarity relationships in the stable boundary layer is

$$\phi_i(\zeta_l) = a_i(1 + b_i\zeta_l)^{c_i} \tag{4}$$

where coefficients a_i, b_i and c_i need to be found experimentally. Accordingly, the non-dimensional wind shear defined as

$$\phi_m(\zeta_l) = \frac{k(z-d)}{u_{*l}}\frac{\partial U}{\partial z} \tag{5}$$

where U is the mean wind speed, is also a unique function of stability. For neutral conditions ($\zeta = 0$), ϕ_m approaches unity. As the exact forms of the similarity functions are not predicted by similarity theory and they should be determined from field experiments, many different formulations have been proposed based on the data from different experiments (e.g. Beljaars and Holtslag, 1991; Cheng and Brutsaert, 2005; Dyer, 1974; Grachev et al., 2007; Sorbjan and Grachev, 2010). We will compare our results to the linear relationship of Dyer (1974) obtained for the stable SL

$$\phi_m(z/L) = 1 + b_m\frac{z}{L} \tag{6}$$

where $b_m = 5$. Högström (1988) modified several existing formulas for ϕ_m (and also for the non-dimensional temperature profile, ϕ_h), in order to comply with his assumptions of $k = 0.4$ and $(\phi_h)_{\zeta=0} = 0.95$. For Dyer's expression (6), he obtained a value $b_m = 4.8$. Additionally, we compare our results to the non-linear stability function of Beljaars and Holtslag (1991)

$$\phi_m(z/L) = 1 + a\frac{z}{L} + b\frac{z}{L}e^{-d\frac{z}{L}} - bd\frac{z}{L}\left(\frac{z}{L} - \frac{c}{d}\right)e^{-d\frac{z}{L}} \tag{7}$$

where $a = 1$, $b = 0.667$, $c = 5$, $d = 0.35$, as expressions (6) and (7) are probably the most often used for parameterization in numerical models. Both relationships were derived over flat and homogeneous terrain using Obukhov length, which is based on surface values. While the first expression was derived and verified by different experiments in the stability range 0 < z/L < 1, Eq. (7) is valid in strongly stable conditions were the overestimation of the non-dimensional gradients is reduced. Linear equations for the stable SL together with the relations for the unstable conditions are traditionally called Businger-Dyer relations (Businger et al., 1971; Dyer, 1974). Similar to the non-dimensional velocity variances we use the non-dimensional wind shear in its local form (see Eq. (5)).

Another widely used stability parameter is the flux Richardson number, defined based on the vertical gradient of wind speed

$$Rf = \frac{-\frac{g}{\theta_v}\overline{w'\theta'_v}}{u_*^2\frac{\partial U}{\partial z}}. \tag{8}$$

Grachev et al. (2013) argued that the upper limit for applicability of the local similarity theory is determined by the inequalities $Ri < Ri_{cr}$ and $Rf < Rf_{cr,}$ where Ri is the gradient Richardson number. They found both critical values to be equal to $Ri_{cr} = Rf_{cr} = 0.20 - 0.25$, with $Rf_{cr} = 0.20 - 0.25$ being the primary threshold. The *z*-less concept requires that *z* cancels in Eqs. (4) and (6). As a result, a linear relationship for the non-dimensional function ϕ_m is obtained, while non-dimensional functions ϕ_i asymptotically approach constant values:

$$\phi_m(\zeta_l) = b_m\zeta_l\ , \tag{9}$$

$$\phi_i = \ b_i\ , \tag{10}$$

where b_m and b_i are experimentally determined coefficients. For convenience, throughout this paper we will use the notation $\zeta = \ \zeta_l$ as all variables are based on local values.

3. Data and Methods

3.1. Site description

A 62 m high tower was located in the vicinity of the small industrial town Kutina, Croatia (tower coordinates: 45°28'32"N, 16°47'44"E). The tower was placed above a grassy surface and it was surrounded by approximately 18 m high black walnut (Juglans nigra) trees. The closest trees are approximately 20−25 m away from the tower and they encompass an area of approximately 120−480 m^2 (Fig. 1). The tower is situated in a rather heterogeneous surrounding regarding both a larger spatial scale (Fig. 1a) and immediate vicinity of the measurement site (on the order of 1 km distance, Fig. 1b). To the east of the tower, crop fields, which extend to the aerial distance of more than 1 km, are found. South-southeast of the tower, about 800 m to 1.5 km distant a large petrochemical industry plant is placed. In a sector that encounters winds from the north-northwest to the northeast, low, forested hills are located. They are covered with a dense forest, while at lower elevations, cultivated orchards and vineyards are found. Foots of these hills are roughly 1.3 km away from the measurement site. Thus, due to different surface roughness features measurements in the SBL at the measuring site may be contaminated by local advective fluxes, drainage flows and/or orographically-generated gravity waves. These features are related to (sub)mesoscale motions which do not obey similarity scaling and are therefore removed from our data by the rigorous data quality control and post-processing options as described later in the paper (Section 3.2.). We are thus focusing on the micrometeorologically complex local site characteristics, which may be more typical for real sites than the usually investigated homogeneous reference sites.

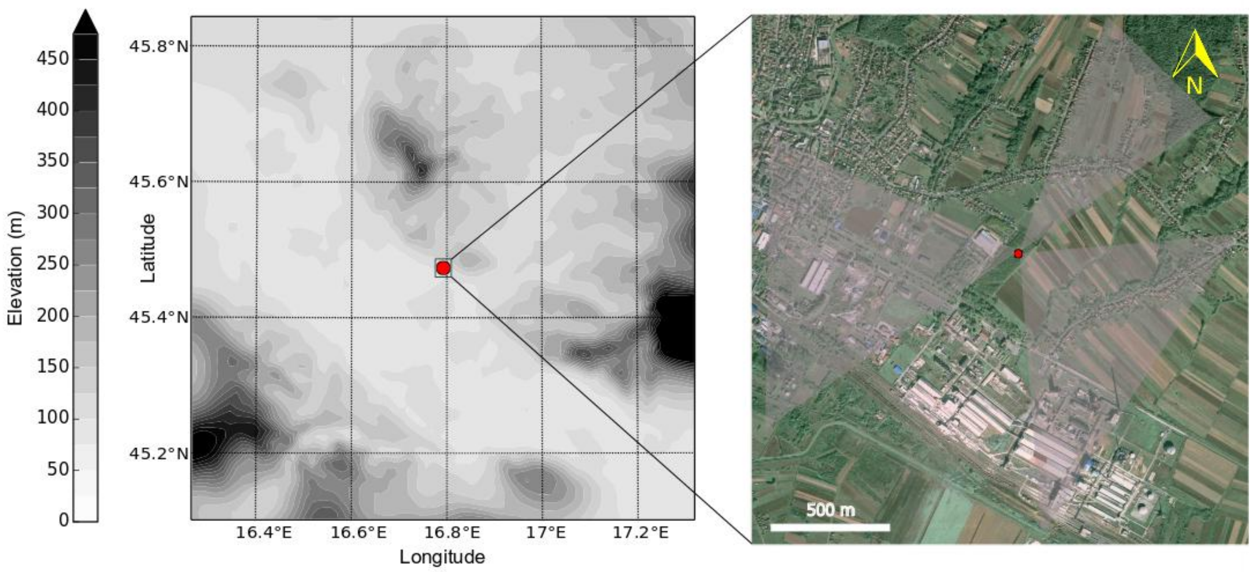

Fig. 1. (a) Topographic map with contour lines each 25 m of the area surrounding the measurement site (red dot) representing inhomogeneous terrain on a larger spatial scale. (b) Google Maps image (Image © 2015 DigitalGlobe) of the observational site. Measurement tower is indicated with a red dot (45°28'32"N, 16°47'44"E). Light gray shaded areas correspond to wind directions depicted in Fig. 5.

Data used in this study were collected during wintertime (1 December 2008−28 February 2009) and correspond to the nocturnal period from 1800 to 0600 local time. Turbulence measurements of three-dimensional wind and sonic temperature were continuously measured using identical WindMaster Pro (Gill Instruments) ultrasonic anemometers that sampled at 20 Hz. Data were measured at five levels above the canopy height, hereafter at level 1 (z_1 = 20 m above the surface), level 2 (z_2 = 32 m), level 3 (z_3 = 40 m), level 4 (z_4 = 55 m) and level 5 (z_5 = 62 m). Measurement levels were prescribed prior to the experiment through existing tower infrastructure. Given the complicated and spatially inhomogeneous characteristics of the measurement site, an idealized vertical structure is considered as a zero-order approach in the analysis. Estimate of vertical layers for neutral conditions was done using different models available in the literature and serves as a simple model for the interpretation of the results. For stably stratified conditions these estimates will not be perfectly appropriate, but will provide the gross picture.

Conceptually, when the air flows over changing terrain, the downwind surface conditions are likely to influence the measurements via internal boundary layers (IBLs), which grow in height (h_i) with downwind distance (Fig. 2) (e.g. Cheng and Castro, 2002; Dellwik and Jensen, 2005). Only the lowest portion of the IBL (10%) is in equilibrium with the new surface (internal equilibrium layer, IEL) while the flow above the IBL is in equilibrium with the upstream surface conditions. The IEL can, finally, be identified with the inertial sublayer (IS). However, if the new surface is very rough its lower part must be considered as a RSL. Within the upper part of the IEL, i.e. IS, turbulent fluxes are approximately constant with height, MOST is valid and the mean wind speed follows the expected logarithmic profile. Within the RSL, the flow is influenced by the distribution and structure of canopy elements (Monteith and Unsworth, 1990; Rotach and Calanca, 2014), with momentum and scalars transported by turbulence, wake effects and molecular diffusion (Malhi, 1996). Above the height of the IEL (h_e) stress and fluxes start to decrease due to the upwind influence. This layer is defined as a transition layer (Fig. 2). Due to the very tall roughness elements we use the zero-plane displacement height (d) as our reference - hence the IBL is assumed to range from $z = d$ up to $z = h_i + d$. Ideally, after a long enough flow over the new surface the IBL fills the entire boundary layer. Since we are interested in evaluating the degree to which local scaling applies under inhomogeneous fetch conditions we map the idealized SBL structure to the IBL. The transition layer then becomes the outer part of the inhomogeneously forced SBL.

We have estimated the length scales introduced above as follows: h_i is estimated based on the model of Cheng and Castro (2002)

$$\frac{\mathrm{h_i}}{\mathrm{z_{02}}} = 10.56\left(\frac{\mathrm{x}}{\mathrm{z_{02}}}\right)^{0.33}, \tag{11}$$

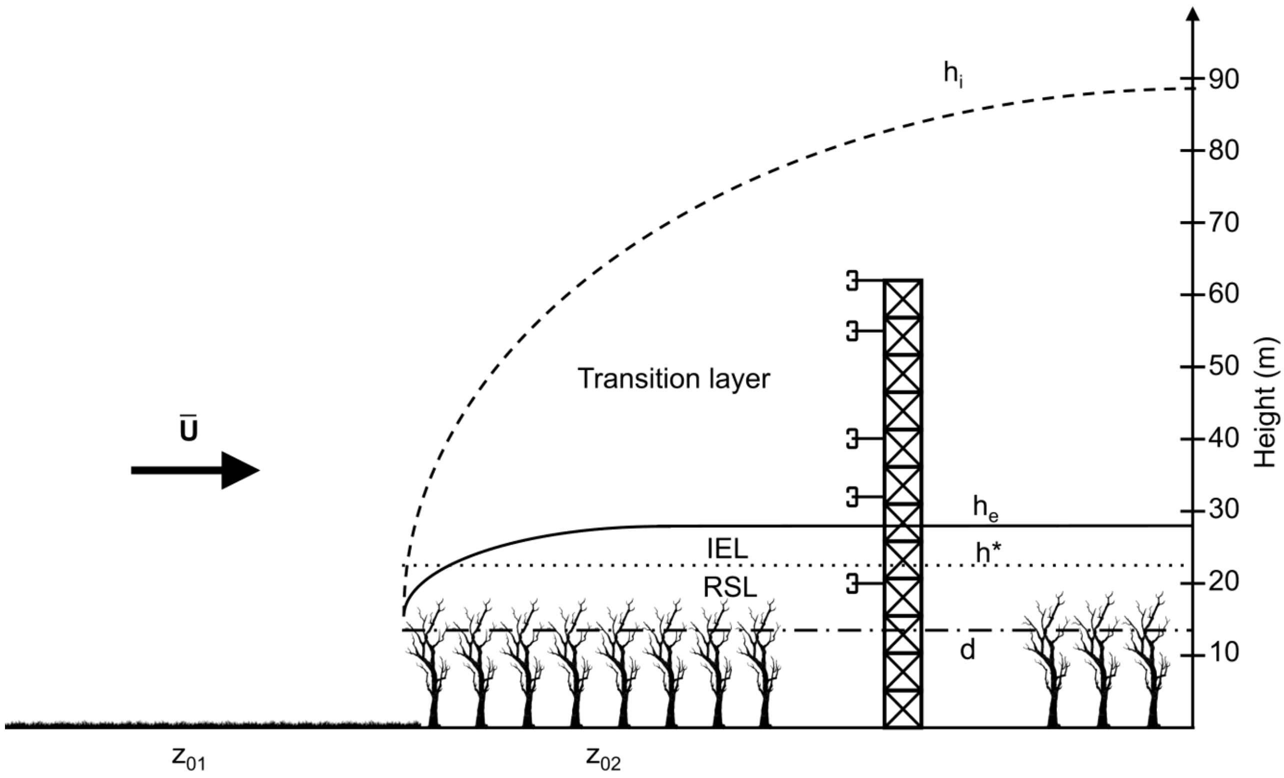

Fig. 2. Conceptual sketch of idealized vertical layers after a step change in surface roughness for the long fetch case (391 m) under neutral conditions. The height of the IBL (h_i), which develops due to the change in roughness conditions, is estimated based on the model of Cheng and Castro (2002). Above the h_i the flow is in equilibrium with the upwind surface. Within the internal equilibrium layer (IEL) the flow is in equilibrium with the forest. The transition layer indicates the transition zone between upwind and downwind equilibrium conditions. The dotted line denotes the height of the RSL, h^*, estimated based on relation of Raupach (1994). The dash-dot line shows the zero-plane displacement height (d) estimated as $3/4h_c$ (Kaimal and Finnigan, 1994; Stull, 1988). z_{01} and z_{02} correspond to upwind and downwind roughness lengths, respectively. The black arrow denotes the mean wind (U) direction.

where x is the distance to the roughness change from the position of measurement (fetch) and z_{02} is the roughness length of the new surface. Following Cheng and Castro (2002), h_e can be determined as

$$\frac{h_e}{z_{02}} = 1.47\left(\frac{x}{z_{02}}\right)^{0.37}. \tag{12}$$

The depth of the RSL (h^*) depends on different properties, such as canopy density, roughness length for momentum and tree height. Raupach (1994) estimated the height of the RSL as

$$\frac{h^*-d}{h_c-d} = 2. \tag{13}$$

For the zero-plane displacement we use a straightforward methodology, $d = \frac{3}{4}h_c$ (Kaimal and Finnigan, 1994; Stull, 1988), where $h_c = 18$ m is the average canopy height, which is estimated through direct measurements (using laser distance meter). Additionally, for the walnut forest we used $z_{02} = 1$ m (the lower value for the roughness length over forest, $z_0 = 1$ m, according to Foken (2008), his Table 3.1).

The estimated height of the IBL at our site (Tab. 1) varied between 40 and 76 m for short (≈56 m) and long (≈390 m) fetch conditions, respectively. Estimated values of h_e at the location of the tower ranged between 6.5 and 13.7 m according to Cheng and Castro (2002) for short and long fetch cases, respectively.

Table 1
Height of the equilibrium layer (h_e) and of the internal boundary layer (h_i) estimated based on the model of the Cheng and Castro (2002) (Eqs. (11) and (12)) for different fetch (*x*) values corresponding to particular wind directions (WD). Note that these heights indicate the height above the displacement height d. In the determination of the fetch length, holes in the forest or corridors of vegetation other than forest were disregarded if their size was small enough.

WD (deg)	30	60	90	120	150	180	210	240	270	300	330	360
x (m)	92	89	69	56	58	77	391	415	110	84	78	105
$\boldsymbol{h_e}$ (m)	7.8	7.7	7.0	6.5	6.6	7.3	13.4	13.7	8.3	7.6	7.4	8.2
$\boldsymbol{h_i}$ (m)	47	46	43	40	40	44	76	77	50	46	44	49

These estimates indicate that the second measurement level is above the IEL height ($z = h_i + d$) for all wind directions. Also, the height of the RSL at our measurement site is $h^* = 1.25h_c$, that is, approximately 22.5 m. Using the above estimates, we find that level 1 is likely to be within the RSL for all wind directions. For cases characterized with the short fetch, the IEL will most likely be within the RSL ($h_e + d < h^*$), while only for wind direction with large fetch conditions (200−250 deg) the growing equilibrium layer will encompass the RSL and a thin IS will form. Levels 2 and 3 are in the transition layer for all wind directions, while levels 4 and 5 are even above h_i for the short fetches (105−175 deg). The highest measurement level reflects the upwind surface conditions for fetches shorter than 100 m. Hence a potential RSL influence should be detectable if level 1 behaves differently. If levels 2−5 do not show different behavior this can be taken as an indication that our crude mapping assumption has some validity.

3.2. Post processing of the data

Instruments were mounted 3 m away from the triangular lattice tower (booms facing to the northeast) to minimize any flow distortion effect by the tower. Considerable loss of data was incurred due to intermittent winter icing or temporary instrument malfunction (Table 2). During this period, light nocturnal winds were common at the site at the lowest measurement level (Fig. 3). We assume that the sonic temperature $T_s = T(1 + 0.51q)$, where T is the air temperature, is close to the virtual potential temperature θ_v. Automated quality control procedures were not used since they may be too strict for the SBL analysis of weak turbulence. Raw 20-Hz data were first divided into 30-min intervals. These intervals were checked for large data gaps, and all 30-min intervals with more than 1% of missing data were omitted from further analyses. After the consistency limits check, where we removed the data having unrealistically high values, spikes (defined as data points within the time series which deviate more than four standard deviations from the median value of the particular 30-min averaging window) were removed. If the number of spikes within the 30-min interval was less than 1% of the total data, spikes were replaced by linear interpolation from neighboring values. We calculated angles of attack for each measurement and for each flux averaging period, and flagged it if angles of attack exceeded 15 deg. The number of 30-min intervals available for the further post-processing is labeled as "minimum QC" (Table 2). A cross-correlation correction of the time series is already implemented in the Gill Instruments software.

Although double rotation of the data is the most commonly used to correct for sonic misalignment, according to Mahrt (2011) and Mahrt et al. (2013) it should not be applied to SBL data under weak-wind conditions. In the very stable boundary layer direction-dependent mean vertical motions may occur where minor surface obstacles can significantly perturb the flow. In a setup like ours characterized by tall vegetation and/or complex terrain, a non-zero 30-min mean vertical wind component may exist. In such situations a planar fit (PF) method (Wilczak et al., 2001) would be better since it is based on an assumption that the vertical wind component is equal to zero only over longer averaging periods. PF method performs a multiple linear regression on the 30-min wind components to obtain the mean streamline plane (Aubinet et al., 2012). This plane is based on the measurements made during the 88-night period for each of five levels (Table 2).

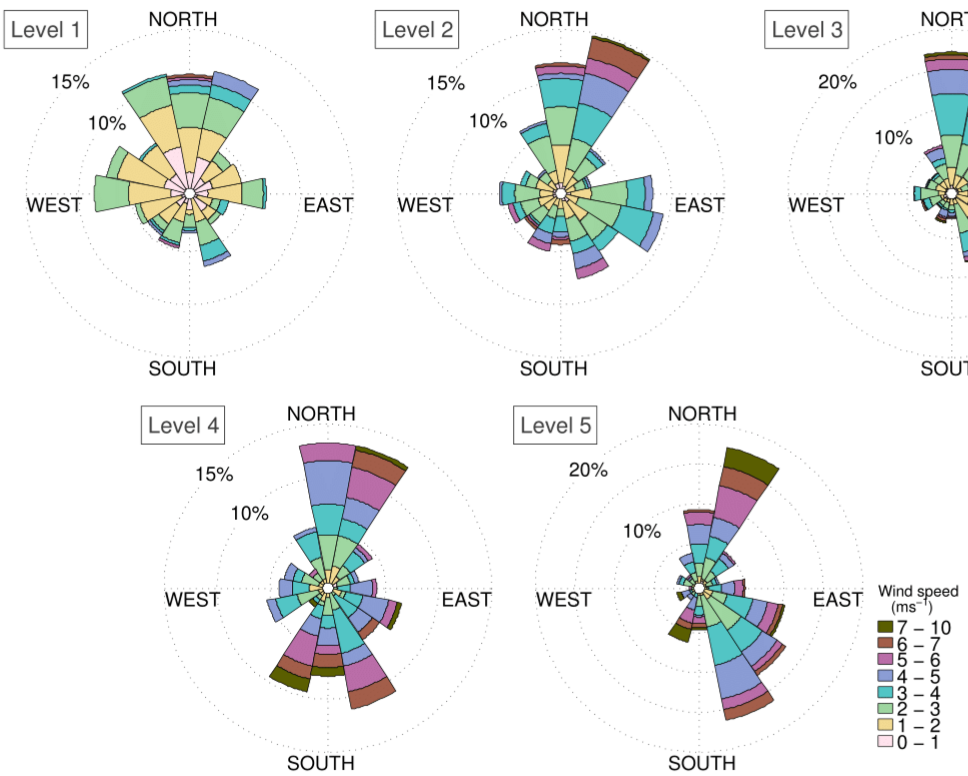

Fig. 3. Wind roses at the measurement site for 30-min averaged data for the analyzed period (December 2008–February 2009). Levels 1 to 5 correspond to measurement heights of 20, 32, 40, 55 and 62 m above the ground, respectively.

Basu et al. (2006) have shown that using an averaging window of inappropriate length can lead to false conclusions concerning the behavior of the turbulence. In stable flows, use of an averaging time that is too large leads to serious contamination of the computed flux by incidentally captured mesoscale motions (Howell and Sun, 1999; Vickers and Mahrt, 2003). Previously Babić et al. (2012) applied two methods based on Fourier analysis to determine an appropriate turbulence averaging time scale. In this study, we have used a multiresolution flux decomposition (MFD) method (Howell and Mahrt, 1997) as described in Vickers and Mahrt (2003). If the gap timescale is employed in the calculation of turbulent fluctuations, contamination by mesoscale motions should be removed. Accordingly, in comparison with the use of an arbitrary averaging time scale, similarity relationships should be improved. Here, based on the MFD method we obtained a gap timescale of 100 sec, which is shorter than the previous value obtained by Babić et al. (2012) for a single night case. Thus, a value of 100 sec was used here for a high-pass filtering of the time series of raw u, v, w and T_s by applying a moving average. Since averaging over a longer time period (i.e. 30 or 60 min) reduces random flux errors in the case of relatively stationary turbulence, turbulent variances and covariances in the present study correspond to 30-min averages. The mean wind speed and wind direction were derived from the sonic anemometer data.

Stationarity of the time series is a fundamental assumption of similarity theory. Thus, it should be tested prior to evaluation of similarity theory. Večenaj and De Wekker (2015) performed a comprehensive analysis to detect non-stationarity based on various tests proposed in the literature. They found that the Foken and Wichura (1996) test most often detects the largest number of non-stationary time intervals among all the tests investigated. They concluded that non-stationarity significantly decreases if detrending or high-pass filtering is applied, since highly non-stationarity (sub)mesoscale motions are removed by filtering. Therefore, while testing non-stationarity of our datasets we first removed the linear trend for each 30-min interval and then applied the Foken and Wichura (1996) test to the filtered time series. The percentage of non-stationary periods for our dataset over heterogeneous terrain in the SBL varied between 20 and 30 % depending on the level of observation (Tabe 2). This is slightly lower compared to studies of complex mountainous terrain of Večenaj and De Wekker (2015) and Stiperski and Rotach (2016).

The statistical uncertainty (or sampling error) is inherent to every turbulence measurement. The assessment of the statistical uncertainty is related to the averaging period. In order to estimate statistical uncertainty we followed Stiperski and Rotach (2016). We performed this test on the time intervals which were declared stationary by the foregoing test. The statistical uncertainty was estimated for the momentum and heat fluxes, and for the variances. This was done for the fixed averaging period of 30-min. Although over ideally flat and homogeneous surfaces one might choose 20% as a limit of statistical uncertainty, we chose the 50% to assure both, high quality data sets, and a significantly large amount of input data for the similarity analysis (Stiperski and Rotach, 2016). Thus, for the subsequent analysis only 30-min intervals associated with statistical uncertainty below 50% were chosen. The uncertainty was largest for the kinematic heat flux while for variances it was on average smaller than 50%.

Finally, following the QC recommendations by e.g. Klipp and Mahrt (2004) and Grachev et al. (2014) we imposed the following thresholds: data with the local wind speed less than 0.2 ms^{-1} were omitted, while minimum thresholds for the kinematic momentum flux, kinematic heat flux, and standard deviation of each wind speed component were 0.001 ms^{-1}, 0.001 Kms^{-1} and 0.04 ms^{-1}, respectively.

Table 2
Number of 30-min intervals that satisfy the minimum QC (no large data gaps, no unrealistic values and no spikes) within the observed period of 88 nights (out of a total of 2112 possible intervals). The number of stationary and also the number of time intervals which are stationary and have uncertainty < 50% (used for the analysis in this study) is given.

Crtieria	Level 1	Level 2	Level 3	Level 4	Level 5
Minimum QC	647	802	1898	564	803
Stationary	482	576	1323	388	649
Stationary & Uncertainty < 50%	342	388	760	225	357

Footprints are estimated and used in order to facilitate an interpretation of the results. Kljun et al. (2015) presented a new parameterization for Flux Footprint Prediction (FFP) which has improved footprint predictions for elevated measurement heights in stable stratification. Furthermore, the effect of the surface roughness has been implemented into the scaling approach. It is based on a scaling approach of flux footprint results of a thoroughly tested Lagrangian footprint model. A two-dimensional flux footprint model of Kljun et al. (2015) (http://footprint.kljun.net/) was used to estimate the surface upwind of the measurement tower that defined the fetch (flux footprint function) for the measurements at each level during stable conditions. As input parameters we used the mean standard deviations of lateral wind component (σ_v = 0.40, 0.45, 0.41, 0.46 and 0.46 ms^{-1} for levels from 1 to 5, respectively), the mean local Obukhov lengths (Λ = 33, 28, 38, 45 and 39 m), the mean friction velocities (u_{*l} = 0.23, 0.20, 0.19, 0.22 and 0.21 ms^{-1}) and correspondingly, mean wind velocity for each measurement height (U = 1.9, 2.9, 3.1, 4.0 and 4.1 ms^{-1}). The height of the SBL was set to 250 m since the result did not exhibit noticeable sensitivity to its choice. The peak location of the footprint function, i.e. location of the maximum influence on the measurement, increases with increasing height and varies between 19 and 405 m from the lowest to the highest observational level, respectively. Additionally, the distance from the receptor that includes 90% of the area influencing the measurement (x_R) increases with height, where $x_R \approx$65, 331, 570, 1260 and 1300 m, correspond to levels 1 to 5, respectively.

3.3. Assesment of self-correlation

Monin-Obukhov as well as local similarity theory leads to self-correlation, because both predicted variables and the predictors are functions of the same input quantities (Hicks, 1978). As an example, prediction of σ_i/u_{*l} (i = u, v, w) or ϕ_m in terms of the stability parameter contains self-correlation since both

σ_i/u_{*l} or ϕ_m and ζ depend on u_{*l}. To test the role of self-correlation in our dataset, we followed the approach of Mahrt (2003) as described in Klipp and Mahrt (2004), using 1000 random samples. Random datasets were created by redistributing the values of σ_u, σ_v, σ_w, u_{*l} and dU/dz from the original dataset for each measurement level. We used threshold values $-\overline{w'\theta'_v} > 0.001$ mKs^{-1} and $dU/dz > 0.001$ s^{-1}, as values less than these are indistinguishable from zero. We repeated this process 1000 times and we calculated corresponding 1000 random linear-correlation coefficients between σ_i and ζ and ϕ_m and ζ. The average of these 1000 random correlation coefficients, $\langle R_{rand}\rangle$, is a measure of self-correlation because random data no longer have any physical meaning. The difference between the squared correlation coefficient of the original dataset R^2_{data} and $\langle R^2_{rand}\rangle$ is proposed as a measure of the actual fraction of variance attributed to the physical process. A very small value of the linear-correlation coefficient (< 0.15) indicates no correlation between compared variables. Mahrt (2014) stated that physical interpretation of results becomes ambiguous when the self-correlation is of the same sign as the expected physical correlation. However, this test does not seem to be appropriate for near-neutral and very stable cases (*z*-less limit), since σ_i/u_{*l} and ϕ_m tend to constant values, resulting in small (or even negative) correlation coefficients (Babić et al., 2016)

4. Results and Discussion

4.1. Flux-variance similarity

Variances of wind velocity components provide important information on turbulence intensity as well as for the modeling of turbulent kinetic energy and transport. In this section we evaluate similarity of scaled standard deviations of wind velocity components. Normalized standard deviations of wind components are plotted as a function of the local stability parameter in Figs. 4 and 6. Figure 4 shows that scatter of the data (gray symbols) increases with increasing height, where standard deviations of 0.27, 0.29, 0.41, 0.36 and 0.34 ms^{-1} correspond to levels from 1 to 5, respectively. Note that the number of data is the largest at level 3. Moreover, after applying strict quality control criteria the scatter is substantially reduced (standard deviations in the range 0.21−0.23 ms^{-1}). This is similar to results of Babić et al. (2016), and opposed to some other studies in complex terrain (e.g. Fortuniak et al., 2013; Nadeau et al., 2013; Wood et al., 2010). Stationary data that exceed our uncertainty threshold of 50% are presented in order to show the influence of small fluxes (which are difficult to measure and hence uncertain) on the scatter of σ_w/u_{*l} (presented as gray symbols in Fig. 4). As seen from Fig. 4, this criterion is crucial for excluding the high values of the scaled vertical wind variance in the strongly stable regime where z-less scaling should be valid. Without this exclusion, an incorrect conclusion on the validity of z-less scaling might be drawn. In the subsequent analysis these data are omitted and individual data as well as bin-averages in all figures correspond to data (namely, wind variances and turbulent fluxes) which satisfy an uncertainty limit < 50%.

To evaluate the similarity of the scaled standard deviations we used the relationship form (4), where a_i, b_i and c_i $(i = u, v, w)$ are free fitting parameters (e.g. Wood et al., 2010). The best-fit coefficients were obtained using a robust least-squares fit of all 30-min data (Table 3). We note that values of fitting parameter a_i (neutral limit) for all three non-dimensional velocity variances are smallest at the lowest measurement level. Also, they are smaller than the canonical values for flat and uniform terrain ($\sigma_u/u_* = 2.39 \pm 0.03, \sigma_v/u_* = 1.92 \pm 0.05, \sigma_w/u_* = 1.25 \pm 0.03,$ Panofsky and Dutton (1984)) which clearly indicates influence of the RSL. This justifies our estimates of the vertical structure and footprints. Turbulence characteristics and transport in this layer are determined by the presence of coherent structures which are generated at the canopy top (e.g. Finnigan and Shaw, 2000; Shaw et al., 2006). These coherent eddies and extra mixing are generated by the inviscid instability mechanism (Raupach et al., 1996). Values of $a_{v,w}$ at levels 2−5 are larger compared to the Panofsky and Dutton (1984) values for the neutral range, while the a_u value for level 2 is larger. For three other levels values are slightly smaller (Table 3). Values of σ_w/u_{*l} larger than 1.25 (value reported for "ideal" flat terrain) are often observed over non-uniform terrain and may be attributed to horizontal momentum transport (Katul et al., 1995).

Table 3
Fitted relationships for non-dimensional standard deviations of wind components. Functional forms (Eq. (4)) of non-dimensional standard deviations of velocity components were tested using a robust least-squares method.

Level	Height*	σ_u/u_{*l}	σ_v/u_{*l}	σ_w/u_{*l}
Level 1	20 m	$2.10(1+7.27\zeta)^{0.09}$	$1.30(1+1506\zeta)^{0.1}$	$0.94(1+656\zeta)^{0.06}$
Level 2	32 m	$2.48(1+0.57\zeta)^{0.12}$	$2.10(1+9\zeta)^{0.1}$	$1.34(1+3.39\zeta)^{0.08}$
Level 3	40 m	$2.32(1+0.15\zeta)^{0.36}$	$2.00(1+1.9\zeta)^{0.1}$	$1.43(1+0.18\zeta)^{0.26}$
Level 4	55 m	$2.24(1+0.79\zeta)^{0.15}$	$1.70(1+6.7\zeta)^{0.1}$	$1.21(1+15.94\zeta)^{0.07}$
Level 5	62 m	$2.13(1+0.75\zeta)^{0.17}$	$2.00(1+0.9\zeta)^{0.2}$	$1.30(1+0.59\zeta)^{0.22}$

* above ground level

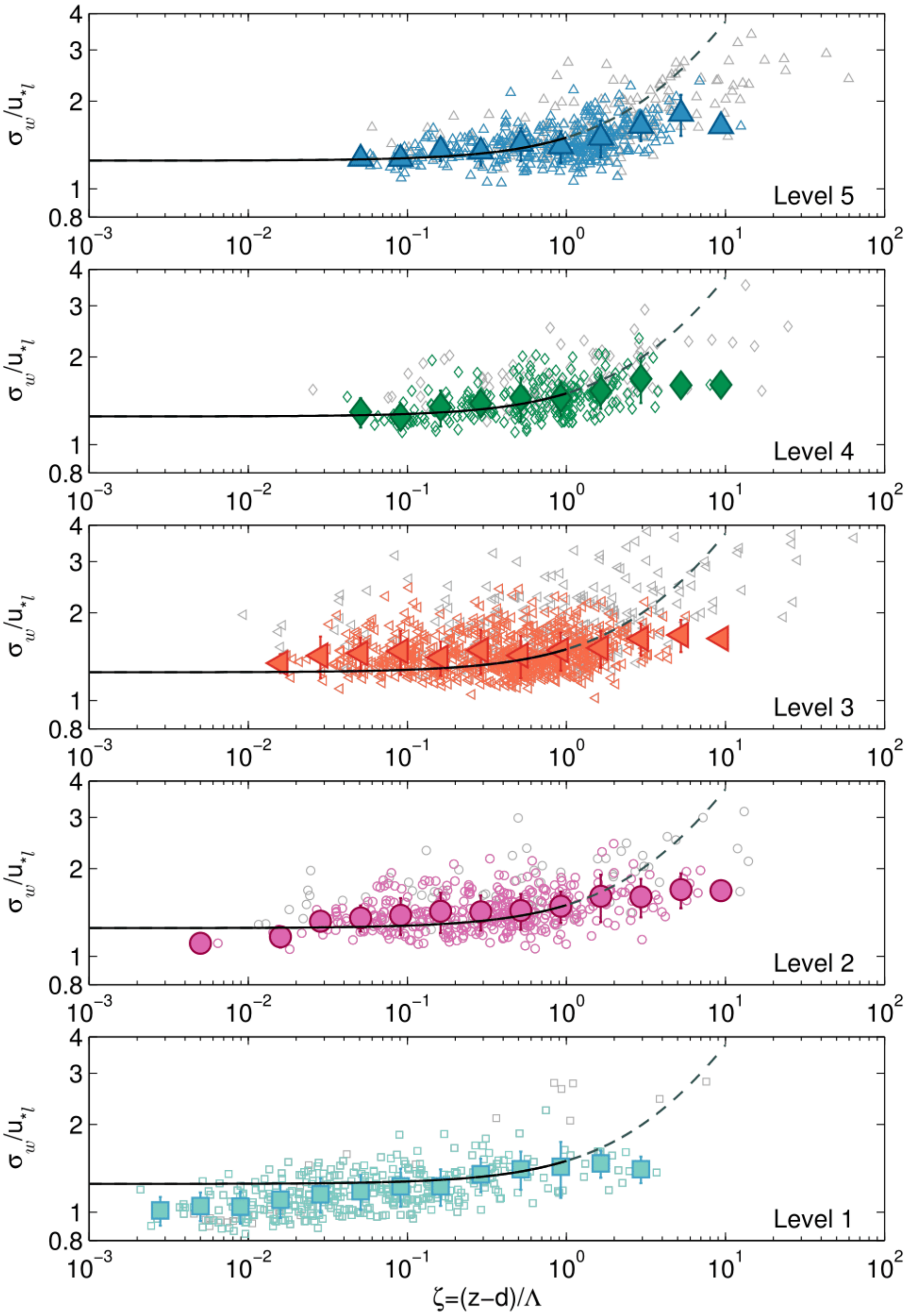

Fig. 4. Scaled standard deviation of vertical velocity fluctuations as a function of stability. Black solid line ($0 < \zeta < 1$) corresponds to: $\phi_w = 1.25(1 + 0.2\zeta)$ (Kaimal and Finnigan, 1994). Thin dashed line is an extension for $1 < \zeta < 10$. Individual data at each level are shown as background symbols (gray symbols represent stationary data points which exceed our uncertainty threshold of 50%). Error bars indicate one standard deviation within each bin. The bin size is determined in a logarithmic scale using fifteen equally spaced bins in the stability range $0.002 < \zeta < 12.5$.

As already mentioned, flux-variance similarity relationships are influenced by self-correlation. Small values of fitted coefficients b_i and/or c_i indicate the best-fit curve which converges to a constant, i.e. a_i. Consequently, values of R^2_{data} tend to converge to small values or even to zero, while $\langle R^2_{rand}\rangle$ are usually larger which leads to negative values of $R^2_{data} - \langle R^2_{rand}\rangle$. The same result was obtained by Babić et al. (2016) and, as they pointed out, this presents a limitation of the method since it relies on the linear correlation coefficient and does not allow for a reliable conclusion about self-correlation in the SBL.

Table 4 presents a review of $\sigma_{u,v,w}/u_{*l}$ published in the literature for different terrain characteristics under neutral conditions. As already noted, dimensionless velocity variances in the RSL often exhibit lower values in comparison with the flat terrain reference of Kaimal and Finnigan (1994). Our results for $\sigma_{u,v}/u_{*l}$ at the lowest measurement level are in the range of values obtained within RSLs over forest (Rannik, 1998) and urban (Rotach, 1993) areas. For levels 2−5, neutral values are close to those reported by Moraes et al. (2005) and Wood et al. (2010). Using local scaling over the city of London (measurements at 190 m above the ground), Wood et al. (2010) obtained near-neutral limits of σ_i/u_{*l} ($i = u, v, w$), which are in accordance with those reported for flat and homogeneous terrain where MOST applies. They concluded that MOST was not complicated by too many factors, since London is quite flat and there are consistent building heights across a wide area which produced a longer upwind fetch causing the London boundary layer likely to be in equilibrium with the surface. Our results for σ_w/u_{*l} are furthermore consistent with Nieuwstadt (1984) who found it to be constant (~ 1.4) in the stability range $0.1 < \zeta < 2$.

Table 4
Comparison of neutral values for non-dimensional standard deviations of the wind from different studies. Our near-neutral values correspond to the mean value of scaled standard deviations of wind in the range $0 < \zeta < 0.05$.

Reference	**Site description**	$\boldsymbol{\sigma_u/u_{*l}}$	$\boldsymbol{\sigma_v/u_{*l}}$	$\boldsymbol{\sigma_w/u_{*l}}$
Panofsky and Dutton (1984)	Flat (reference)	2.39 ± 0.03	1.92 ± 0.05	1.25 ± 0.03
Rotach (1993)	Urban RSL	2.2	1.5	0.94
Rannik (1998)	Pine forest RSL	2.25 ± 0.31	1.82 ± 0.29	1.33 ± 0.14
Moraes et al. (2005)	Complex (valley)	2.4	2.2	1.2
Wood et al. (2010)	Urban BL	2.36	1.92	1.40
This study – Level 1	Heterogeneous	2.13	1.65	1.11
This study – Levels 2−5	Heterogeneous	2.41	2.08	1.37

4.1.1. Influence of the surface heterogeneity

Due to the fact that measurements were performed in a very heterogeneous landscape, we investigated possible influences of different land-use types on turbulence statistics by considering changes for different wind directions. Figure 5a shows the normalized standard deviation of the vertical wind component for each observational level averaged over the entire stability range plotted versus wind direction. For the wind sector 45−90 deg there is no consistent increase of σ_w/u_{*l} with height, possibly due to the fact that this narrow wind sector is characterized through a sudden change of surface roughness (from agricultural fields to rough forest) and also through a short fetch (some 70 m). This might indicate a more complex vertical structure than depicted in Fig. 2 with flow which has not reached equilibrium yet. In the 300−360 deg wind sector, the non-dimensional variance of the vertical wind has decreased values at the highest level in comparison with values at levels 2−4. We hypothesize that this might indicate an influence of drainage flows from hills located north of the measurement site. Drainage flows are thermally-driven and they occur during night over sloping terrain often leading to the formation of low level jets. However, we do not have the necessary information to substantiate this hypothesis. In the 190 − 260 deg sector, σ_w/u_{*l} increases with height indicating the flow which has adjusted to the new surface. This sector has the longest fetch (over 300 m) and highly rough but uniform underlying surface (Figs. 1 and 2).

Observed changes of the normalized vertical wind variance with varying wind direction reflect the influence of the surface inhomogeneity (and possibly topography). This influence is seen from the ratio of observed non-dimensional variance of the vertical wind and corresponding values of commonly used similarity formulas for σ_w/u_{*l} in the "ideal" HHF terrain (e.g. Kaimal and Finnigan (1994), σ_w/u_{*l} = 1.25(1 + 0.2ζ)) in the stability range 0 < ζ < 1 (Fig. 5b). We observe that ratio of these two similarity functions at the lowest measurement level is typically less than one, except for the flow from sectors 200−220 deg and 300−340 deg, which correspond to high roughness and long fetch (Fig. 1) and high wind speeds (Fig. 3), respectively. At upper levels values of the ratio $\phi_w/\phi_{w(HHF)}$ are larger than unity for wind azimuth ranges 55−80 deg, 170−230 deg and 300−360 deg (Fig. 5b). For these levels, the average $\phi_w/\phi_{w(HHF)}$ ratio in Fig. 5b varies between 0.96 and 1.33, which is similar to values obtained by Rannik (1998) in the study over a forest, and the standard deviation for 10 deg wide bins is between 0.08 and 0.22.

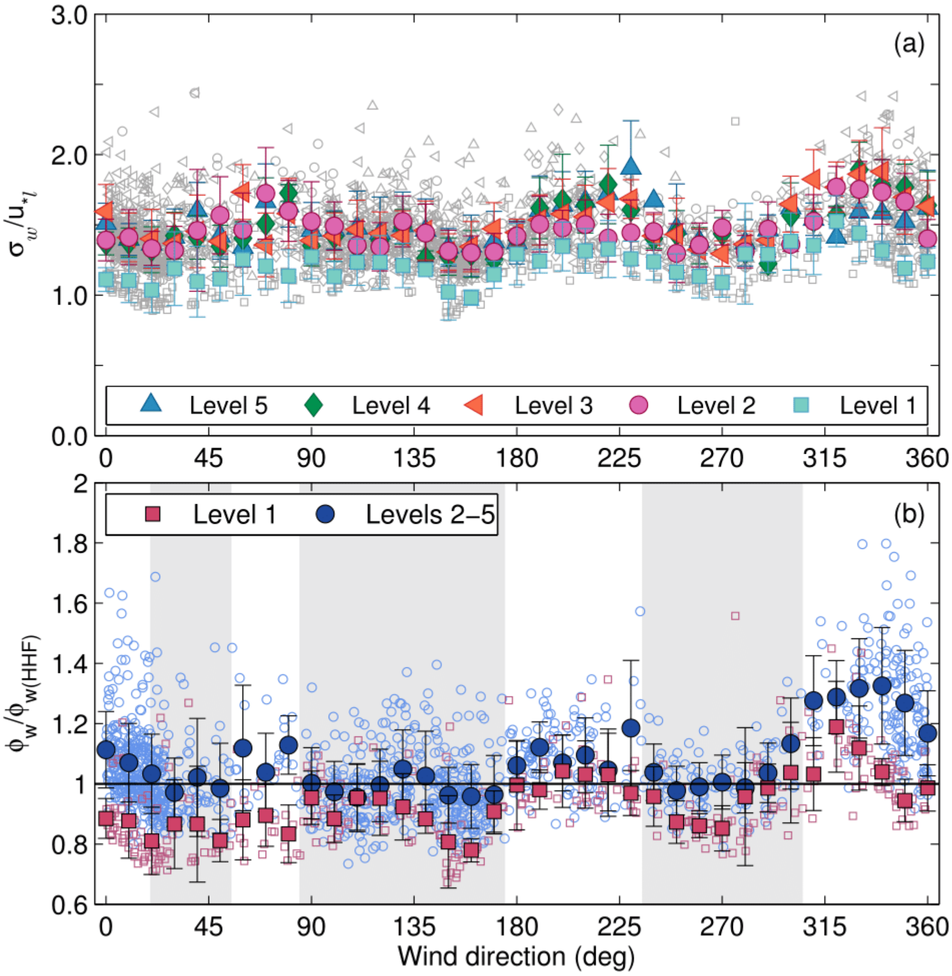

Fig. 5. (a) Scaled standard deviation of vertical velocity fluctuations as a function of wind direction (regardless of stability). Individual data points at each level corresponding to the particular wind sector are shown as background symbols. Colored filled symbols correspond to bin averages over the entire stability range at each observational level. Error bars indicate one standard deviation within each bin. (b) Observed dimensionless standard deviation of vertical wind speed (for the lowest level and levels 2−5) relative to the SL similarity prediction for HHF terrain (Kaimal and Finnigan (1994), denoted "HHF") for stability $0 < \zeta < 1$, plotted versus wind direction. Shaded light gray areas indicate the wind azimuths which correspond to undistorted surface conditions ($\phi_w/\phi_{w(HHF)} \approx 1$). These correspond to wind directions 20−55 deg, 85−175 deg and 235−295 deg. The flow from other wind directions is considered as distorted.

Accordingly, we separately analyzed the velocity variances for different wind directions corresponding to undistorted and distorted sectors, respectively. Based on $\phi_w/\phi_{w(HHF)} \approx 1$ undistorted wind directions were defined to correspond to wind directions 20−55 deg, 85−175 deg and 235−295 deg (light gray shaded area in Fig. 5b). All other wind directions were considered as distorted. The number of data within each group was nearly evenly distributed except for the highest level. Namely, the percentage of data corresponding to the undistorted sectors was 47, 56, 54, 52 and 64 % for levels from 1 to 5, respectively.

Figure 6 shows all three non-dimensional standard deviations at the lowest level and for levels 2−5 for undistorted and distorted wind direction sectors separately. We note that the scatter is larger for horizontal components than for the vertical wind component. Also, as one might expect the scatter is larger for the distorted sectors compared to undistorted. Normalized variances at level 1 show much less dependence on the wind direction compared to levels 2−5. This reflects the rather local RSL impact that determines the statistics. That is, RSL turbulence appears to be affected by a fetch of less than 100 m from the tower as was estimated by the flux-footprint model (Section 3.2.) rather than by the more distant complex surface. Differences between distorted and undistorted sectors at this level are only found in the near-neutral regime with larger magnitudes for the distorted sectors. For levels 2−5 we observe that the overall shape of the curves for the two sectors is quite similar for all three wind variances. Dimensionless longitudinal and vertical wind variances show higher values in the distorted sectors, while the lateral wind variance seems to be independent on the wind direction. Similar to level 1, the lateral wind component shows a more pronounced increase with stability than the longitudinal and vertical variances. The dimensionless vertical wind variance in the undistorted sectors can be represented quite well with the similarity relationship valid for flat and homogeneous terrain (Kaimal and Finnigan, 1994) in the stability range $0.01 < \zeta < 1$. Based on modeled footprints particular wind sectors were related to corresponding surface types, accordingly. For the undistorted wind directions 20 − 55 deg and 85 − 175 deg the underlying surface is represented with agricultural fields, while the 235−295 deg sector represents somewhat rougher but quite uniform surface covered mostly with the forest (Fig. 1). This implies that measurements at levels 2−5 corresponding to these sectors correspond to a layer which is in equilibrium with the underlying surface of more uniform roughness. In the strongly stable regime (for $\zeta > 1$) the normalized variances show a tendency for a leveling-off , thus suggesting that *z*-less scaling might be appropriate. This implies that even for highly inhomogeneous terrain local scaling appears to be appropriate for all three velocity variances and that the local Obukhov length is relevant length scale. Additionally, in the strong stability limit the *z*-less scaling seems to be appropriate for longitudinal and vertical wind variances.

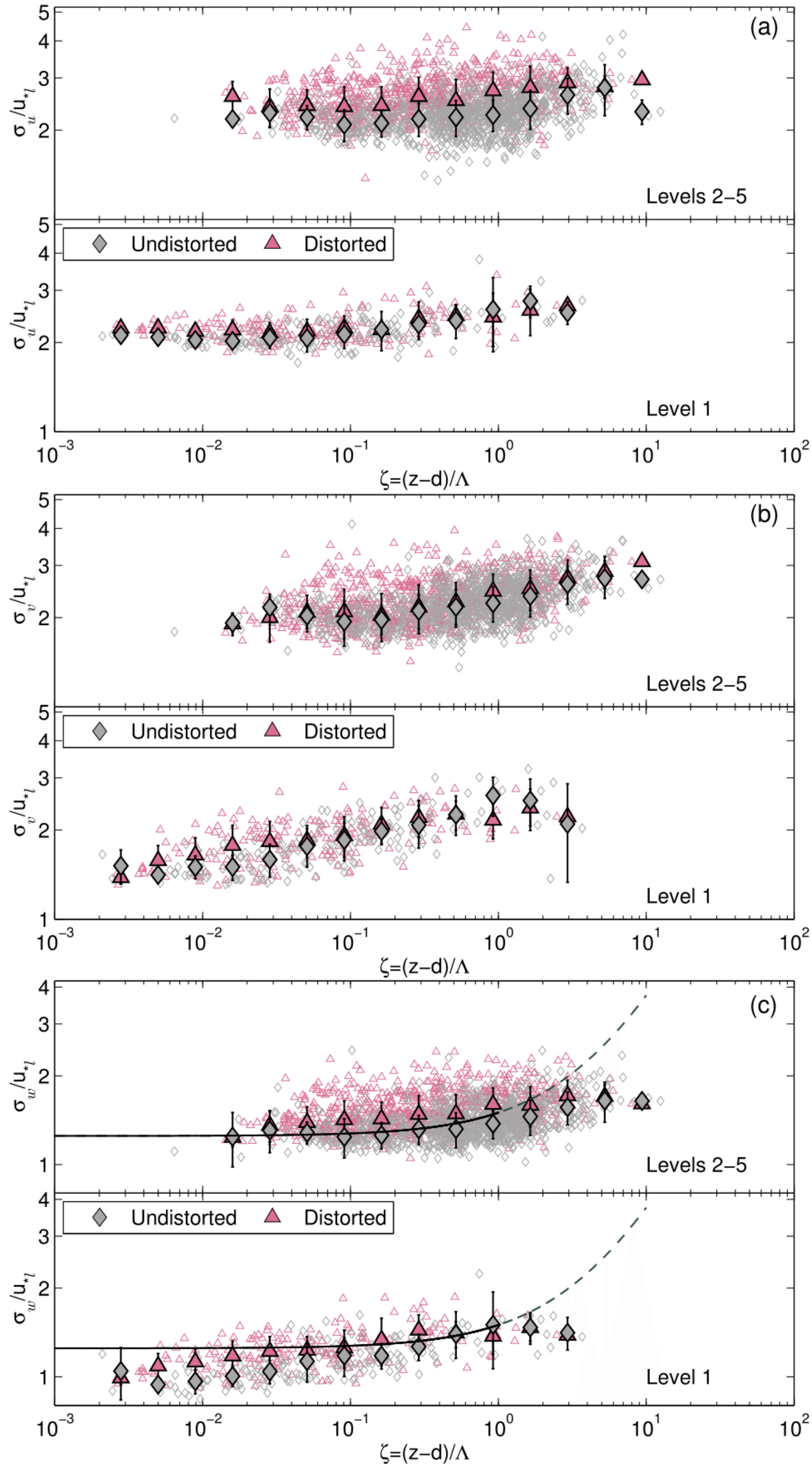

Fig. 6. Scaled standard deviations of (a) longitudinal, (b) lateral and (c) vertical velocity fluctuations as functions of stability for level 1 (lower sub-panels) and levels 2−5 (upper sub-panels) for distorted (pink triangles) and undistorted (gray diamonds) wind sectors. For explanation of other symbols see Fig. 4.

4.1.2. Subcritical and supercritical turbulence regimes

Grachev et al. (2013) showed that the inertial subrange, associated with the Richardson-Kolmogorov cascade, dies out when both the gradient and the flux Richardson number exceed a “critical value” of approximately $0.20 - 0.25$, with $Rf_{cr} = 0.20 - 0.25$ being the primary threshold. They argued that a collapse of the inertial subrange is caused by the collapse of energy-containing/flux-carrying eddies. This leads to the invalidity of Kaimal's spectral and cospectral similarity (Kaimal, 1973) and consequently, to violations of flux-profile and flux-variance similarity. Correspondingly, Grachev et al. (2013) classified the traditional SBL into two major regimes: subcritical and supercritical. In the former ($Ri < Ri_{cr}$ and $Rf < Rf_{cr}$), turbulence statistics can be described by similarity theory and it is associated with Kolmogorov turbulence. The supercritical regime ($Ri > Ri_{cr}$ and $Rf > Rf_{cr}$) is related to small-scale, decaying, non-Kolmogorov turbulence, and strong influence of the Earth's rotation even near the surface. Figure 7 shows the dependence of Rf (Eq. (8)) on the local stability parameter at the measuring site. Dyer's parameterization (Dyer, 1974) predicts an asymptotic limit to Rf_{cr}= 0.2 (solid black line), but this under-predicts Rf for higher stabilities for which Rf increases above Rf_{cr} = 0.25 (supercritical regime). The range of stability available for our analysis of the profile data is $0 < \zeta < 5$. For example, at levels 4 and 5, 40% and 50% of data points have $Rf > Rf_{cr}$, respectively. Thus, higher levels, which correspond to higher stabilities, are characterized by non-Kolmogorov turbulence.

Grachev et al. (2013) have found that $Rf_{cr} = 0.20$ was the primary threshold for σ_w/u_{*l}. The normalized standard deviation of the vertical wind speed was reported to become asymptotically constant in the subcritical regime indicating consistency with *z*-less scaling in this regime. In the supercritical regime σ_w/u_{*l} was monotonically increasing with increasing stability. The turbulence characteristics at our site (exemplified by the vertical velocity variance, Fig. 8) do not show a clear distinction in behavior between sub- and supercritical regimes as was found in Grachev et al. (2013) and for the non-dimensional vertical gradient of mean wind (Fig. 12). In the subcritical regime the number of data points at levels 2−5 with $\zeta > 1$ is equal to 25 and is represented by only two bin averages. While Grachev et al. (2013) had a much broader range of stability in both regimes (they obtained z/Λ as small as 0.02 for the supercritical and up to 5 for the subcritical regime, respectively), in our dataset the results for these two regimes are almost indistinguishable (Fig. 8). Additionally, for the supercritical regime Grachev et al. (2013) observed an

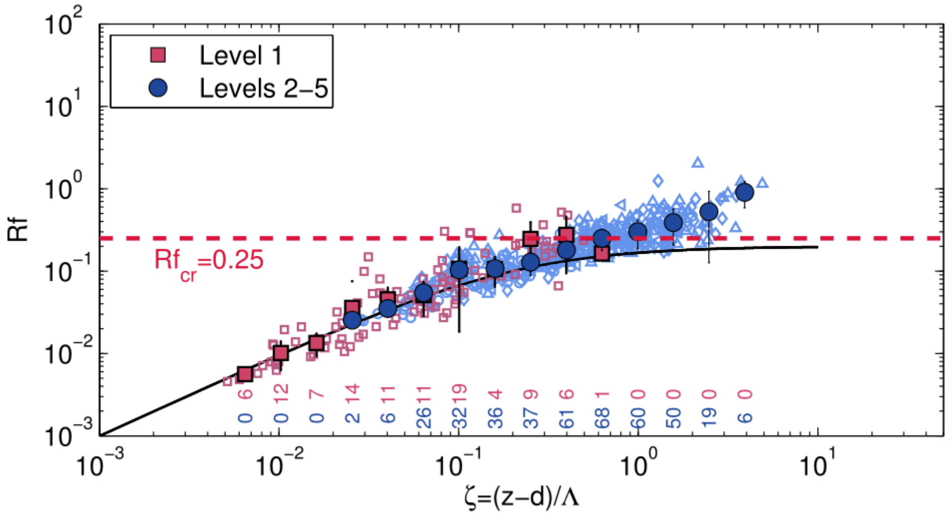

Fig. 7. Stability dependence of the flux Richardson number for all five levels (shown with corresponding symbol). Red squares and blue circles denote bin averages for the lowest level and for levels 2−5, respectively. Error bars indicate one standard deviation within each bin. Number of data points inside each bin for the two subsets of the data is also given.

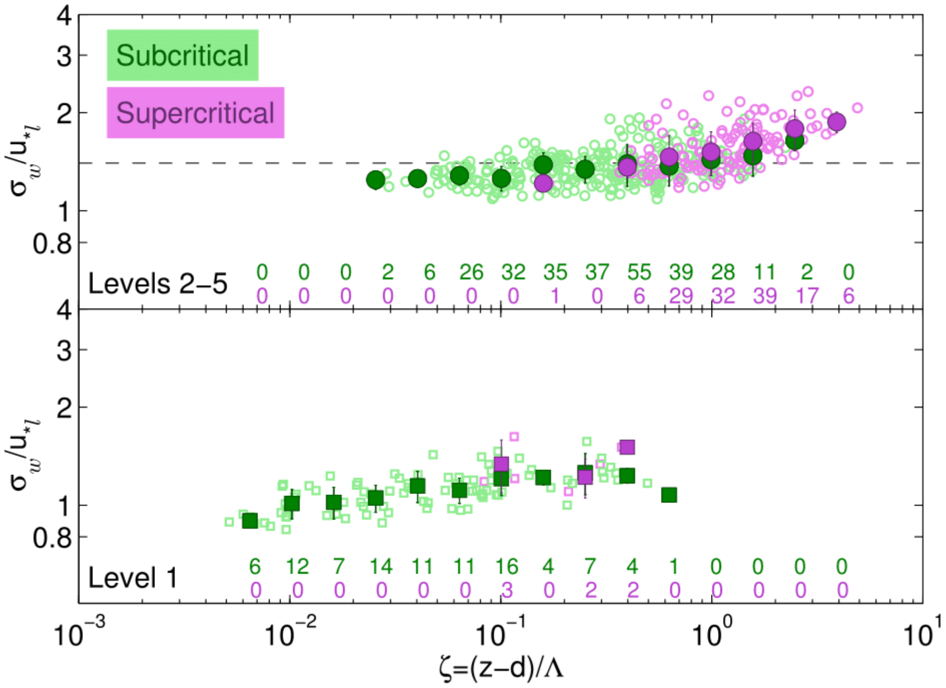

Fig. 8. Scaled standard deviation of vertical velocity fluctuations as a function of stability. Data from the lowermost level (squares) and for levels 2−5 (circles) in the subcritical (green) and supercritical (violet) regime are presented. The dashed line is equal to 1.4 which is the mean value of all data for levels 2−5 in the subcritical regime. The number of data in each regime is indicated with the corresponding color.

increase of σ_w/u_{*l} in the range $3 < \zeta < 100$. For this regime we observed an increasing tendency for the two highest levels, but this is probably not significant because of the small number of data and a restricted stability range (upper limit is ζ = 5). Note that the number of data points here is much less compared to Figs. 4 and 6 because only 100 simultaneous 30-min intervals were available for the calculation of the flux Richardson number. Similar results are found for the horizontal wind variances (not shown).

4.2. Turbulent kinetic energy

Estimation of turbulent kinetic energy (TKE) is very important for atmospheric numerical modeling, since turbulent mixing is often parameterized using TKE. Here we investigate the TKE, defined as, $e = \frac{1}{2}\left(\overline{u'^2} + \overline{v'^2} + \overline{w'^2}\right)$, which represents a turbulent kinetic energy per unit mass (Stull, 1988). Fig. 9 shows *e* scaled by the squared friction velocity. In numerical models which use 1.5-order closure or TKE closure, TKE is predicted with a prognostic energy equation, and eddy viscosity is specified using the TKE and some length scale. Since TKE is essentially the sum of variances (divided by 2), according to Kansas values for neutral conditions (Kaimal and Finnigan, 1994), the value of scaled TKE is equal to 5.48 for HHF terrain.

Over HHF terrain in Antarctica, Sanz Rodrigo and Anderson (2013) found that for neutral to moderate stabilities non-dimensional TKE is roughly constant up to ζ = 0.5. Above this value, non-dimensional TKE grows until it reaches ζ = 10 (corresponding to the boundary-layer top), which is followed by an asymptotic value for stronger stabilities (Fig. 9, dashed black line, Eq. (14)). They proposed a simple empirical parameterization:

$$\frac{TKE}{u_{*l}^2}(\zeta) = \begin{cases} \frac{1}{\alpha_0} + b_E\zeta\,, & \zeta \leq 10 \\ \frac{1}{\alpha_0} + b_E 10\,, & \zeta > 10 \end{cases} \tag{14}$$

where $\alpha_0 = 0.22$ is the neutral limit value and $b_E = 0.5$.

We fitted the above linear relation to our data from levels 2−5 in the stability range 0.006 < ζ < 8.30 (Fig. 9, orange dashed line) using the least-squares method. Figure 9 shows a clear influence of the RSL on the lowest measurement level, which does not correspond to the proposed near-linear expression (14). The RSL influence also results in a reduced value of non-dimensional TKE for the neutral range ($TKE/u_{*l}^2 \approx$ 4.25 based on values from Tab. 4) in comparison with the value of 4.5 found by Sanz Rodrigo and Anderson (2013). Their value is smaller than the reference value of 5.48 for HHF terrain probably due to higher air density in the Antarctica causing reduced values of TKE/u_*^2 compared to mid-latitudes. We note that the relation of the type given by Eq. (14) fits our data for levels 2−5 quite well (Fig. 9, orange dashed curve), but with slightly different coefficients $\alpha_0 = 0.16$, which corresponds to a neutral value of $TKE/u_*^2 = 6.1$, and $b_E = 0.8$. The fitted neutral value of dimensionless TKE for levels 2−5 is close to the value of 6.01, which is obtained based on values from Tab. 4.

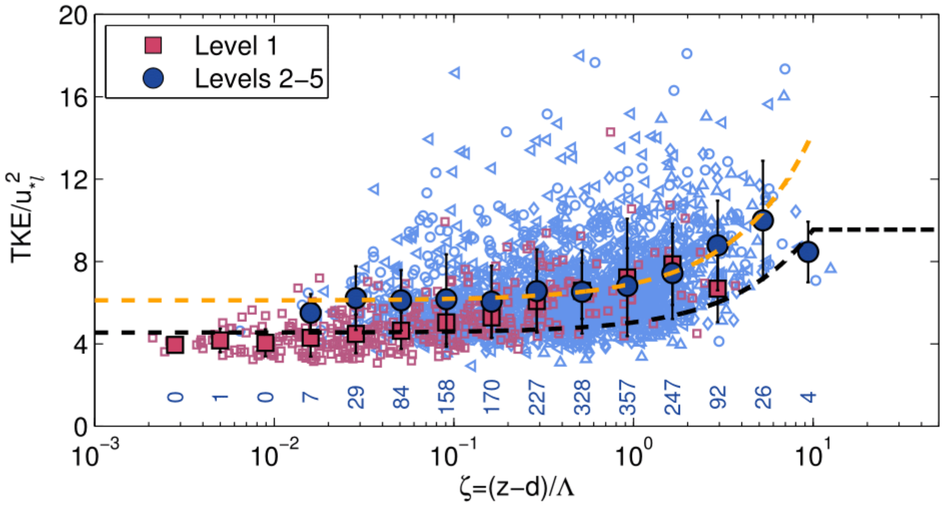

Fig. 9. Dependence of non-dimensional turbulent kinetic energy on stability. The black dashed line is an empirical fit (Eq. (14), Sanz Rodrigo and Anderson (2013)). Individual data at each level are shown in background symbols, while red squares and blue circles represent bin-averages for the lowest and four higher levels, respectively. Error bars indicate one standard deviation within each bin. The number of data points within each bin for levels 2−5 is also indicated. The orange curve is a fit to our data for levels 2−5.

Similar to wind variances, analysis of the TKE with respect to wind direction shows similar distinction between the distorted and undistorted sectors. While values of normalized TKE are similar for the two sectors at the lowest level, at levels 2−5 magnitudes in the distorted sectors are larger. The dependence of TKE/u_{*l}^2 on the stability parameter can be represented with a linear relationship, but the best fit coefficients are somewhat changed: $\alpha_0 = 0.19$ and 0.14 and $b_E = 0.97$ and 0.95 for undistorted and distorted sectors, respectively (not shown). The behavior of the normalized TKE in the sub- and supercritical regime was found to be consistent with the behavior of the normalized wind variances and no discernible difference between these two regimes was observed (not shown).

4.3. *Correlation coefficients*

In order to estimate fluxes from mean wind and temperature as inputs for dispersion models it is useful to use turbulent correlation coefficients. These coefficients are a measure of the efficiency of turbulent transfer and are defined as

$$r_{uw} = \frac{\overline{u'w'}}{\sigma_u \sigma_w} \tag{15}$$

$$-r_{wT} = \frac{\overline{w'\theta'_v}}{\sigma_w \sigma_{\theta_v}} \tag{16}$$

where r_{uw} and r_{wT} are correlation coefficients for momentum and heat transfer, respectively. Figure 10 shows momentum and heat flux correlation coefficients estimated for the lowest and the four higher measurement levels. For strong stratification we obtained smaller values of the correlation coefficients for momentum, but they increase quite steeply while approaching neutral conditions. This was also observed in both an urban (e.g. Wood et al., 2010) and a rural dataset (e.g. Conangla et al., 2008). Additionally, r_{uw} exhibits the same behavior with respect to the stability when analyzed for different wind azimuths. The magnitude of the momentum correlation coefficient is larger for the undistorted sector compared to distorted in the stability range $0 < \zeta < 1$ in the whole measurement layer (not shown). The stability-averaged momentum flux correlation coefficient values are between 0.23 and 0.46 at level 1 (Fig. 10a) and a similar range was observed for undistorted (0.22−0.51) and distorted (0.25−0.45) wind sectors. These values are similar to those obtained by Marques Filho et al. (2008). For levels 2−5, the values of r_{uw} are somewhat smaller compared to level 1 and are in the range 0.14−0.34 (Fig. 10a), and they are similar to those obtained for the distorted wind sectors: 0.16−0.31 (not shown), which is in the range of values observed over generally rougher urban surfaces (Wood et al., 2010).

The correlation coefficient for heat exhibits larger values for $\zeta > 0.1$ for levels 2−5, and it decreases while approaching neutral conditions. The correlation coefficient for heat is between 0.10 and 0.26, which is similar to values reported in other studies (Marques Filho et al., 2008; Wood et al., 2010). Additionally, no discernible dependence on wind direction was found for r_{wT} mostly due to the large scatter of the data (not shown). Mean values of the momentum and heat flux correlation coefficients over the entire measurement layer, and for all stabilities, are equal to 0.26 and 0.24, respectively. Also, no discernible difference in behavior of the momentum and heat flux correlation coefficients was observed between the sub- and supercritical regimes (not shown).

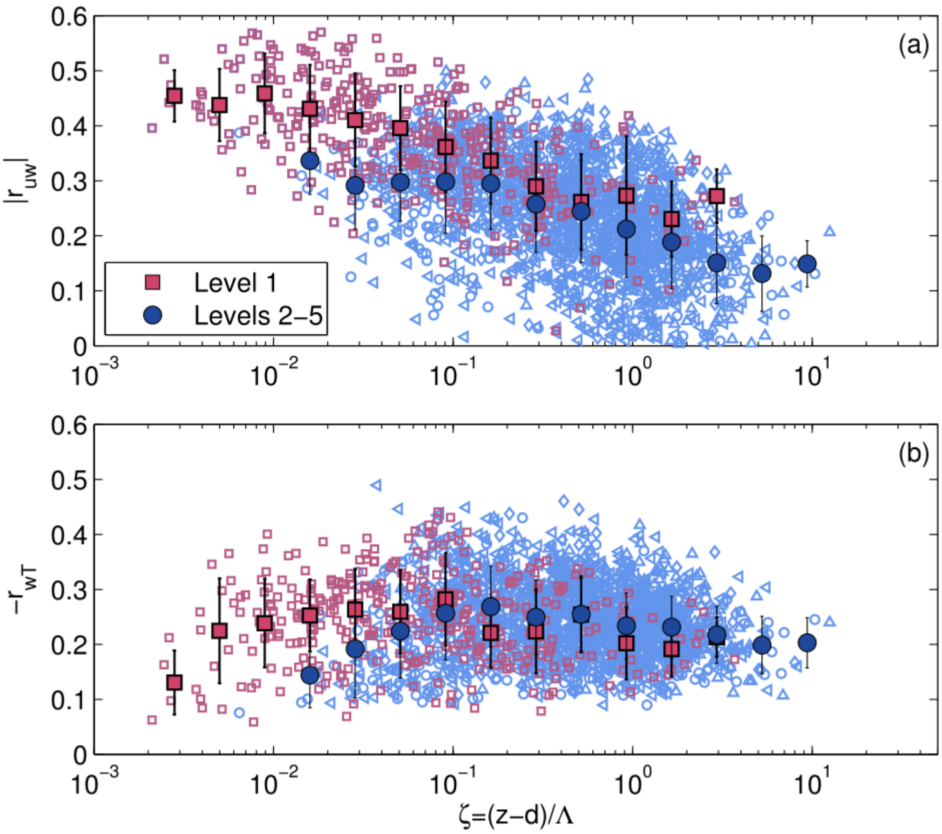

Fig. 10. Momentum (a) and heat flux (b) correlation coefficients plotted as a function of stability. Background symbols represent individual data at each level while red squares and blue circles show bin-averages for the first level and for levels 2−5, respectively. Error bars indicate one standard deviation corresponding to the particular bin.

4.4. Flux-gradient similarity

We also investigated the relationship between mean vertical gradients and turbulent fluxes, also known as the flux-gradient relationships. Several interpolation methods were tested in order to determine the mean wind profile, and the second order polynomial fit was found to best fit the observed data. Thus, the vertical gradient of mean wind speed is obtained by fitting a second order polynomial through the 30-min measured profiles

$$U(z) = p_1 \left[\ln\left(\frac{z-d}{z_0}\right)\right]^2 + p_2 \ln\left(\frac{z-d}{z_0}\right) + p_3 \tag{17}$$

and by evaluating a derivative with respect to z for each measurement level. The second order polynomial fit is widely used for measurements within the roughness sublayer (e.g. Dellwik and Jensen, 2005; Rotach, 1993) as well as within the inertial sublayer (e.g. Forrer and Rotach, 1997; Grachev et al., 2013). Only about one hundred simultaneous 30-min intervals were available from each measurement level for the profile analysis. Results of the variance and TKE analyses showed a different behavior of the first level in comparison with all the others. In order to investigate whether there is a difference in the flux-gradient relationship as well, the data from the first level and levels 2−5 are presented separately (Fig. 11). For our dataset no discernible difference of ϕ_m between level 1 and levels 2−5 can be observed. Almost all data at the first measurement level are within the stability range $z/\Lambda < 0.5$ and ϕ_m tends to a constant value of 1 when approaching near-neutral conditions. Quite diverse results concerning the value of ϕ_m in the RSL in the near-neutral conditions can be found in the literature. While in some studies of flux-gradient similarity within the forest RSL, ϕ_m was found to be less than unity in the near-neutral range (e.g. Högström et al., 1989; Mölder et al., 1999; Raupach, 1979; Thom et al., 1975), other studies indicate that ϕ_m is close to unity (e.g. Bosveld, 1997; Simpson et al., 1998; Dellwik and Jensen, 2005; Nakamura and Mahrt, 2001). Bosveld (1997) found that momentum and heat eddy diffusivities differ in magnitude in neutral conditions. This means that, with increasing canopy density, heat exchange remains enhanced in the RSL, whereas momentum exchange approaches surface-layer values. Dellwik and Jensen (2005) observed an increase of ϕ_m in the RSL in neutral conditions over fetch-limited deciduous forest due to the increased wind gradients directly above the canopy top. In previous studies reporting $\phi_m < 1$ and having mostly been conducted over pine forests (which compared to a closed deciduous forest have less biomass in the top of the canopy) the observed wind profile close to the three tops was less steep.

The previous sections have revealed clear differences in the flux-variance relationships between level 1 and levels 2-5 (i.e., the RSL and the transition layer, respectively) at the present site. In contrast, no significant difference is observed for the flux-gradient relationship. Similar results were reported by Katul et al. (1995) who pointed out that inhomogeneity in the RSL impacts variances but not necessarily fluxes. Following this line, our results seem to indicate that surface characteristics at our site are influencing the strength of turbulent mixing and the wind gradient in the same way. This conclusion is additionally corroborated by the results of the analysis for different wind sectors as no dependence on the wind direction was found for the non-dimensional gradient of wind speed (not shown).

According to Fig. 11, ϕ_m increases more slowly with increasing stability than predicted by the linear approach (Eq. (6), dashed black line) and it appears to closely follow the Beljaars-Holtslag function (Eq. (7)). The Beljaars-Holtslag formulation reduces the overestimation of the non-dimensional gradients for very stable conditions (Fig. 11, black solid line). Similar results were also obtained by other studies. For example, Mahrt (2007) found that ϕ_m increases linearly only up to 0.6, while in the range $0.6 < \zeta < 1.0$ it increases more slowly than the linear prediction. However, according to Grachev et al. (2013) this result brings into question z-less scaling. Assuming that ϕ_m is a linear function of stability, the gradients should tend to constant values for $\zeta \gg 1$. Thus, the leveling-off of the ϕ_m at large stabilities is an evidence for the breakdown of z-less stratification. Grachev et al. (2013) hypothesized that the leveling-off of ϕ_m functions for strong stability may be due to including data for which local similarity is not applicable into the analysis.

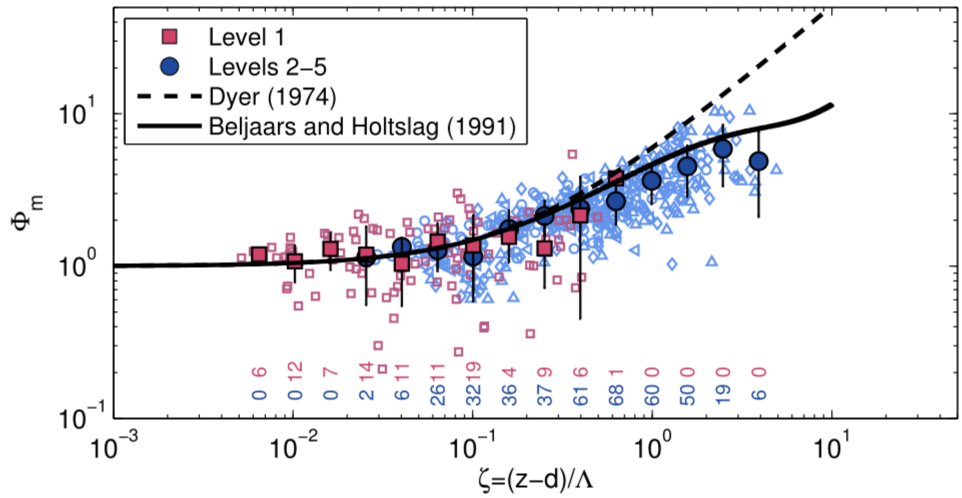

Fig. 11. Non-dimensional vertical gradient of the wind speed plotted versus the local stability parameter. Individual data points for each level are shown in the corresponding symbol (as in Fig. 4), while data from the lowest level are indicated with red color and from levels 2−5 in blue color. Dashed line corresponds to the linear relationship of Dyer (1974)(Eq. (6)) and the solid line is Beljaars and Holtslag (1991) relationship (Eq. (7)). Bin averages for the lowest and four higher levels are included for easier interpretation of results. Error bars indicate one standard deviation within each bin. Number of data points in each bin is also shown.

Following the approach of Grachev et al. (2013), we imposed the prerequisite $Rf < Rf_{cr} = 0.25$ on all individual data at each level. According to Fig. 12, data with $Rf < 0.25$ almost perfectly follow the linear dependence on stability (according to Eq. (6)) with the best-fit coefficient $b_E = 3.8$ (thin dashed line in Fig. 12). This implies the consistency of the data with the z-less prediction. The behavior of the non-dimensional gradient of wind speed in the supercritical regime in Fig. 12 exhibits a large deviation from the linear similarity prediction in the entire stability range. Moreover, supercritical data have a tendency to level-off. This suggests that the Beljaars-Holtslag non-linear expression (Eq. (7), Beljaars and Holtslag, 1991), as well as the results from other studies which exhibited leveling-off of similarity functions (e.g. Baas et al., 2006; Forrer and Rotach, 1997; Grachev et al., 2013, 2007) were most likely affected by a large number of small-scale, non-Kolomogorov turbulence data.

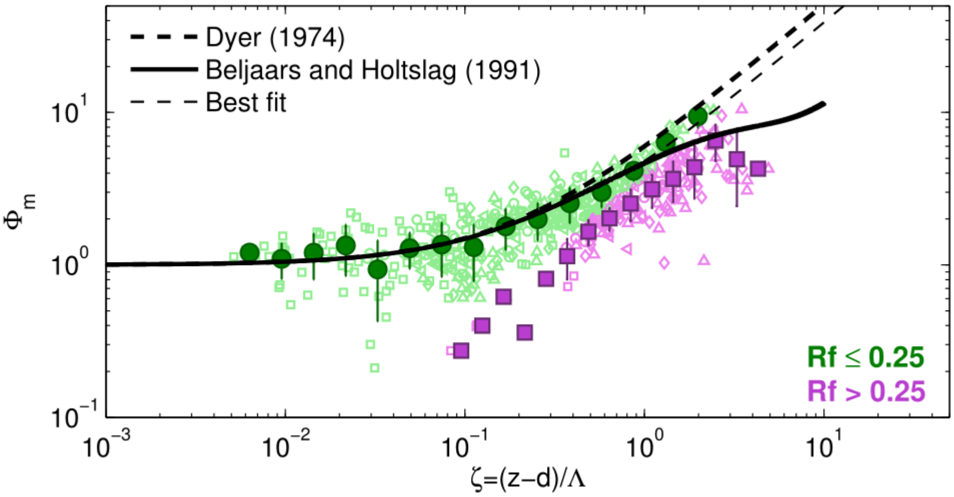

Fig. 12. The non-dimensional vertical gradient of wind speed plotted versus stability for two different regimes: subcritical ($Rf \leq 0.25$, green) and supercritical ($Rf > 0.25$, violet). Error bars indicate one standard deviation within each bin. Thick dashed line indicates the linear relationship (6) (Dyer, 1974); the thin dashed line is the best fit to our data for $Rf \leq 0.25$ (in the stability range $0.005 < \zeta < 2.43$), while the bold solid line corresponds to Eq. (7) (Beljaars and Holtslag, 1991).

Ha et al. (2007) evaluated surface layer similarity theory for different wind regimes in the nocturnal boundary layer based on the CASES-99 data. They concluded that although the stability parameter is inversely correlated to the mean wind speed, the speed of the large-scale flow has an independent role on the flux-gradient relationship. For strong and intermediate wind classes, they found that ϕ_m obeyed existing stability functions when z/L is less than unity, while for weak mean wind and/or strong stability ($z/L > 1$) similarity theory broke down. Following their approach, we evaluated the flux-gradient relationship separately for different wind regimes, which were classified based on the mean wind speed at each level similarly as in the study of Ha et al. (2007), and discriminated between subcritical and supercritical regimes. The striking difference of the behavior of ϕ_m with stability for different wind classes, which was found in the study of Ha et al. (2007), cannot be observed in our dataset (Fig. 13). In the weak wind regime the scatter is largest, although we have noted substantial scatter even for the intermediate and strong classes, caused by the small scale turbulence, which survived even in the supercritical regime (violet symbols). If we consider only data for $Rf \leq 0.25$, they follow Dyer's linear prediction even for the weak wind regime, indicating that similarity theory holds in this regime for the whole range of stabilities.

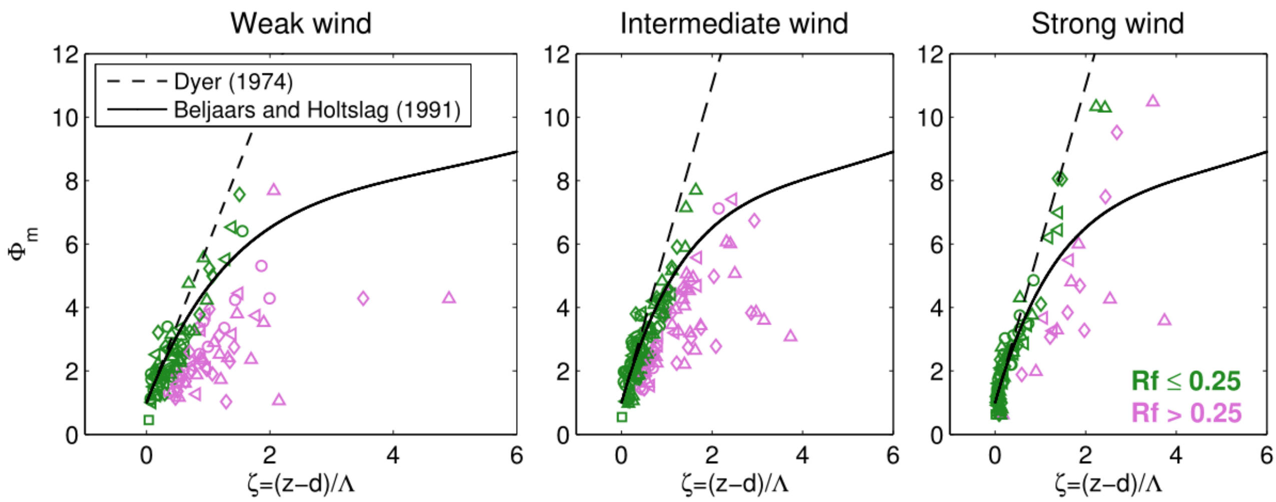

Fig. 13. Non-dimensional vertical gradient of wind speed for each level plotted versus local stability parameter for weak-, intermediate- and strong wind regimes, respectively. Individual data points for each level are shown with the corresponding symbol. Data points exceeding critical value of $Rf_{cr} = 0.25$ (supercritical regime) are shown in violet. Dashed line indicates the linear relationship of Dyer (1974) (Eq. (6)) and the solid line corresponds to the relationship (7) (Beljaars and Holtslag, 1991).

We now turn to the self-correlation analysis. Since the present data exhibit different behavior for the subcritical and supercritical regimes, the self-correlation analysis was performed separately for each of these regimes. Linear correlation coefficients between ϕ_m and ζ for the original data and random data sets were calculated for each level. Table 5 shows the impact of self-correlation on the dimensionless wind shear. Generally, the results for both the sub- and supercritical regimes suggest a non-negligible but not decisive impact of self-correlation. There are, however, two exceptions. At the lowest level, the subcritical data mostly reflect the near-neutral range where large scatter of the data is present resulting in a relatively small correlation coefficient of 0.54. Hence the self-correlation test, which is based on linear correlation, produces small correlations of similar magnitudes for both physical and random data. This in turn results in a very small value of $R^2_{data} - \langle R^2_{rand} \rangle$ which means that results of this test are not very conclusive. At level 5, the correlation coefficient is large in the subcritical regime and reduced in the supercritical due to the increased scatter of the data for ζ > 1.5 in this regime. Consequently, the value of $R^2_{data} - \langle R^2_{rand} \rangle$ is small. For the three middle levels, R_{data} has similar values in both the subcritical and supercritical regime, since in both regimes they exhibit a strong positive fit, i.e. ϕ_m increases with increasing stability with the larger scatter observed at level 4 (Fig. 12).

Table 5
Self-correlation analysis. R_{data} is a linear correlation coefficient between ϕ_m and ζ for the original data at each level. $\langle R_{rand} \rangle$ is the self-correlation and it is the average of the correlation coefficients for 1000 random datasets. $R^2_{data} - \langle R^2_{rand} \rangle$ is a measure of the true physical variance explained by the linear model as proposed by Klipp and Mahrt (2004). Standard deviations are also indicated. N is the number of 30-min intervals.

Subcritical	**N**	R_{data}	$\langle R_{rand} \rangle$	$\sigma\langle R_{rand} \rangle$	$R^2_{data} - \langle R^2_{rand} \rangle$	$\sigma(R^2_{data} - \langle R^2_{rand} \rangle)$
Level 1	93	0.54	0.51	0.14	0.01	0.14
Level 2	83	0.91	0.55	0.11	0.50	0.12
Level 3	78	0.95	0.49	0.11	0.64	0.11
Level 4	60	0.73	0.49	0.13	0.28	0.13
Level 5	52	0.97	0.49	0.14	0.68	0.13
Supercritical						
Level 1	7	0.91	0.68	0.22	0.33	0.25
Level 2	17	0.91	0.51	0.18	0.54	0.18
Level 3	22	0.92	0.55	0.18	0.51	0.19
Level 4	39	0.66	0.43	0.15	0.22	0.13
Level 5	48	0.57	0.41	0.14	0.14	0.12

Grachev et al. (2013) proposed a new method which is not influenced by self-correlation and for which *z*-less scaling should also be valid. This new function represents a combination of universal functions and is thus a universal function itself. This new function,

$$\phi_m \phi_w^{-1} = 0.75(1 + 5\zeta) \tag{18}$$

where the value of $\phi_w = 1.33$ corresponds to the median value in the subcritical regime found in the study of Grachev et al. (2013) (Fig. 14, gray solid line). For our data, the median ϕ_w value for levels 2−5 was also found to be equal to 1.33 in the subcritical regime. According to Fig. 14a, the increase of $\phi_m \phi_w^{-1}$ with stability is slower than the linear prediction (solid and dashed lines, respectively). Due to the fact that this new similarity function $\phi_m \phi_w^{-1}$ shares no variable with the stability parameter (except the reference height *z*−*d*), the observed decrease below the linear prediction is not caused by self-correlation. As seen from Fig. 14b, this deviation from the linear relationship is mainly due to the small scale turbulence in the supercritical regime ($Rf > 0.25$). Additionally, this function is consistent with the z-less scaling when the prerequisite $Rf \leq 0.25$ is imposed on the data (Fig. 14b). As already noted, the RSL shows a more pronounced influence on the ϕ_w profile compared to the wind shear profile, thus leading to an overestimation of Eq. (18) at level 1 while no systematic deviation can be observed for levels 2−5 (Fig. 14). The scatter in the near-neutral range at level 1 could be partly due to the wind direction inhomogeneities (not shown).

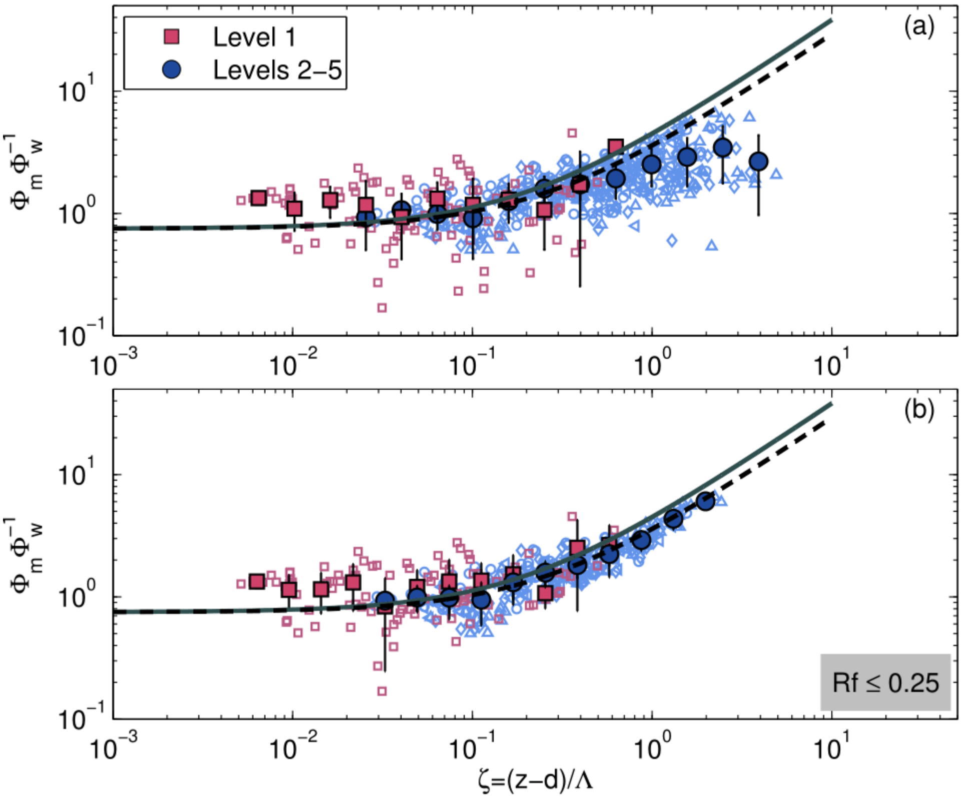

Fig. 14. The bin-averaged non-dimensional function $\phi_m \phi_w^{-1} = \frac{k(z-d)}{\sigma_w} \frac{dU}{dz}$, which is not influenced by self-correlation, plotted versus local stability. Individual data for each level are shown in the corresponding symbol as in Fig. 4. Bin averages for the lowest level (red squares) and four higher levels (blue circles) are included for easier interpretation of trends. Error bars indicate one standard deviation within each bin. Gray line corresponds to the experimental fit according to Grachev et al. (2013) ($\phi_m \phi_w^{-1} = 0.75(1 + 5\zeta)$) and the dashed black line is the best fit to our data ($\phi_m \phi_w^{-1} = 0.75(1 + 3.8\zeta)$) in the subcritical regime. (b) Same as (a) but subject to the condition $Rf \leq 0.25$.

5. Summary and Conclusions

Multi-level measurements of atmospheric turbulence carried out over a heterogeneous surface in the continental part of Croatia have been used to study turbulence characteristics in the wintertime nocturnal boundary layer. Measurements that were obtained from five levels in the layer between 20 and 62 m above the ground and $2-44$ m above the local canopy height, provided valuable insight in the turbulence characteristics within tens of meters above the ground level. We focused on evaluating the applicability of local similarity scaling approach, in terms of flux-variance and flux-gradient similarity, over spatially inhomogeneous surface characteristics.

Due to specific local terrain characteristics and distinctive features of the stable boundary layer (SBL), special attention was given to data quality control and post-processing options, which included determination of appropriate turbulence averaging time scale for defining turbulence fluctuations, testing the stationarity of the data and invoking an uncertainty test. Observations were conducted inside (the lowest observational level) and above the roughness sublayer (RSL).

After removing highly uncertain data points (uncertainty threshold > 50 %), when assessing scaling under inhomogeneous fetch conditions in the SBL, dimensionless standard deviations of wind velocity components were found to behave differently than the dimensionless wind shear. Concerning the normalized standard deviations, it was found that vertical velocity shows a tendency to “ideal” behavior, that is, it follows *z*-less scaling when approaching large stability. The longitudinal and transversal components show a dependency on stability, with the latter exhibiting a more pronounced linear increase with increasing stability. Consequently, scaled turbulent kinetic energy was found to have a linear dependence on the stability parameter in the range $0.05 \leq \zeta \leq 10$ for levels above the RSL. However, we found local scaling to be valid for all three variables, which is astonishing given the complex and spatially inhomogeneous surface characteristics. For neutral conditions, due to the RSL influence values of all three non-dimensional velocity variances were found to be smaller at the lowest measurement level, while these were larger at higher levels in comparison with values obtained for HHF terrain.

The ratio of the observed dimensionless standard deviation of the vertical wind component and corresponding values of commonly used similarity formulas over horizontally homogeneous and flat (HHF) terrain showed considerable variation with wind direction, indicating the influence of surface roughness changes and topography. Therefore, we separately analyzed velocity variances for different wind directions corresponding to undistorted ($\phi_w/\phi_{w(HHF)} \approx 1$) and distorted ($\phi_w/\phi_{w(HHF)} \neq 1$) sectors, respectively. Differences between these sectors at the lowest level were only found in the near-neutral regime with larger magnitudes for the distorted sectors. At upper levels, dimensionless longitudinal and vertical wind variances also showed higher values for these wind directions. However, this did not influence results regarding the relationship with stability. For non-dimensional velocity variances, and consequently non-dimensional TKE and the momentum and heat flux correlation coefficients, no discernible difference between sub- and supercritical regimes was observed.

Results for the non-dimensional wind shear appear to be less sensitive to inhomogeneous site characteristics. Despite the largely inhomogeneous surface characteristics at the measuring site, flux-gradient relationship showed a similar distinction between Kolmogorov and non-Kolmogorov turbulence as found under ideal (HHF) conditions (Grachev et al., 2013). Our results support the classical Businger-Dyer linear expression for the non-dimensional profile of wind speed, with slightly different best-fit coefficient, even over inhomogeneous terrain but only after removing data which correspond to the flux Richardson number $Rf > 0.25$. Hence, our data follow local *z*-less scaling for the ϕ_m function when the condition $Rf = 0.25$ is imposed. Similar to HHF conditions, supercritical ($Rf > 0.25$) data show a leveling-off for ϕ_m at higher stability thus seemingly supporting the non-linear relationship of Beljaars and Holtslag (1991). Therefore, we conclude that the non-dimensional wind shear over a largely heterogeneous vegetated surface is only weakly, if at all, affected by the surface inhomogeneity. Thus, when interested in only subcritical, fully turbulent conditions, the classical linear formulation for ϕ_m is appropriate. Correspondingly, if all turbulence states (regardless of sub- or supercritical) are of interest, the Beljaars-Holtslag formulation is to be preferred. Finally, we investigate whether the wind magnitude has an impact on the distinction between Kolmogorov and non-Kolmogorov turbulence. The flux-gradient dependence on stability did not show different behavior for different wind regimes, indicating that the stability parameter is sufficient predictor for flux-gradient relationship.

Overall, the present stable night-time results from a forested site with highly inhomogeneous fetch conditions show that flux-variance relationships obey local scaling but the corresponding non-dimensional functions do not exhibit the same parameter values as over HHF terrain. The *z*-less limes for strong stability is assumed by the vertical and to somewhat lesser degree by the horizontal velocity fluctuations. The RSL influence appears to be larger than the distortion due to inhomogeneous surface conditions. Flux-gradient relationships, on the other hand, seem to be less influenced by surface inhomogeneity: they exhibit the same distinction into sub- and supercritical turbulence regimes as over HHF terrain. For both, subcritical turbulence alone and “all conditions” the data follow quite closely the respective functions from the literature. Finally, no distinct impact of the RSL can be observed for the flux-gradient relations.

Acknowledgements: We would like to acknowledge Željko Večenaj's crucial role in the setting up instruments and maintenance of the measurement site. We are also thankful for his assistance in the application of MFD and stationarity analysis. We are grateful to Branko Grisogono for providing two sonic anemometers for the use in this experiment. We gratefully acknowledge two anonymous reviewers whose comments led to the improvement of the manuscript. The study was supported by the Croatian Ministry of Science, Education and Sports (grant No. 119-1193086-1323). The first author's research visit at Institute of Atmospheric and Cryospheric Sciences, University of Innsbruck was supported by the Austrian Federal Ministry of Science, Research and Economy (BMWFW) through Ernst Mach Grant – Worldwide program.

References

Andreas, E.L., Hill, R.J., Gosz, J.R., Moore, D.I., Otto, W.D., Sarma, A.D., 1998a. Statistics of surface-layer turbulence over terrain with metre-scale heterogeneity. Boundary-Layer Meteorol. 86, 379–408. doi:10.1023/A:1000609131683

Aubinet, M., Vesala, T., Papale, D., 2012. Eddy Covariance: A Practical Guide to Measurement and Data Analysis. Springer.

Baas, P., Steeneveld, G.J., van de Wiel, B.J.H., Holtslag, A.A.M., 2006. Exploring self-correlation in flux-gradient relationships for stably stratified conditions. J. Atmos. Sci. 63, 3045–3054. doi:10.1175/JAS3778.1

Babić, K., Klaić, Z.B., Večenaj, Ž., 2012. Determining a turbulence averaging time scale by Fourier analysis for the nocturnal boundary layer. Geofizika 29, 35–51.

Babić, N., Večenaj, Ž., De Wekker, S.F.J., 2016. Flux–variance similarity in complex terrain and its sensitivity to different methods of treating non-stationarity. Boundary-Layer Meteorol. 159, 123–145. doi:10.1007/s10546-015-0110-0

Basu, S., Porté-Agel, F., Foufoula-Georgiou, E., Vinuesa, J.F., Pahlow, M., 2006. Revisiting the local scaling hypothesis in stably stratified atmospheric boundary-layer turbulence: An integration of field and laboratory measurements with large-eddy simulations. Boundary-Layer Meteorol. 119, 473–500. doi:10.1007/s10546-005-9036-2

Beljaars, A.C.M., Holtslag, A.A.M., 1991. Flux parameterization over land surfaces for atmospheric models. J. Appl. Meteorol. doi:10.1175/1520-0450(1991)030<0327:FPOLSF>2.0.CO;2

Bosveld, F.C., 1997. Derivation of fluxes from profiles over a moderately homogeneous forest. Boundary-Layer Meteorol. 84, 289–327. doi:10.1023/A:1000453629876

Bou-Zeid, E., Parlange, M.B., Meneveau, C., 2007. On the parameterization of surface roughness at regional scales. J. Atmos. Sci. 64, 216–227. doi:10.1175/JAS3826.1

Businger, J.A., Wyngaard, J.C., Izumi, Y., Bradley, E.F., 1971. Flux-profile relationships in the atmospheric surface layer. J. Atmos. Sci. doi:10.1175/1520-0469(1971)028<0181:FPRITA>2.0.CO;2

Calaf, M., Higgins, C., Parlange, M.B., 2014. Large wind farms and the scalar flux over an heterogeneously rough land surface. Boundary-Layer Meteorol. 153, 471–495. doi:10.1007/s10546-014-9959-6

Cheng, H., Castro, I.P., 2002. Near-wall flow development after a step change in surface roughness. Boundary-Layer Meteorol. 105, 411–432. doi:10.1023/A:1020355306788

Cheng, Y., Brutsaert, W., 2005. Flux-profile relationships for wind speed and temperature in the stable atmospheric boundary layer. Boundary-Layer Meteorol. 114, 519–538.

Cheng, Y., Parlange, M.B., Brutsaert, W., 2005. Pathology of Monin-Obukhov similarity in the stable boundary layer. J. Geophys. Res. Atmos. 110, D06101. doi:10.1029/2004JD004923

Conangla, L., Cuxart, J., Soler, M.R., 2008. Characterisation of the nocturnal boundary layer at a site in Northern Spain. Boundary-Layer Meteorol. 128, 255–276. doi:10.1007/s10546-008-9280-3

de Franceschi, M., Zardi, D., Tagliazucca, M., Tampieri, F., 2009. Analysis of second-order moments in surface layer turbulence in an Alpine valley. Q. J. R. Meteorol. Soc. 135, 1750–1765. doi:10.1002/qj.506

Dellwik, E., Jensen, N.O., 2005. Flux–Profile relationships over a fetch limited beech forest. Boundary-Layer Meteorol. 115, 179–204. doi:10.1007/s10546-004-3808-y

Derbyshire, S.H., 1995. Stable boundary layers: Observations, models and variability part I: Modelling and measurements. Boundary-Layer Meteorol. 74, 19–54.

Dyer, A.J., 1974. A review of flux-profile relationships. Boundary-Layer Meteorol. 7, 363–372. doi:10.1007/BF00240838

Finnigan, J., 2000. Turbulence in plant canopies. Annu. Rev. Fluid Mech. 32, 519–571. doi:10.2480/agrmet.20.1

Finnigan, J.J., Shaw, R.H., 2000. A wind-tunnel study of airflow in waving wheat: an EOF analysis of the structure of the large-eddy motion. Boundary-layer Meteorol. 96, 211–255. doi:10.1023/A:1002618621171

Foken, T., 2008. Micrometeorology. Springer-Verlag Berlin Heidelberg.

Foken, T., Wichura, B., 1996. Tools for quality assessment of surface-based flux measurements. Agric. For. Meteorol. 78, 83–105.

Forrer, J., Rotach, M.W., 1997. On the turbulence structure in the stable boundary layer over the greenland ice sheet. Boudary-Layer Meteorlogy 85, 111–136.

Fortuniak, K., Pawlak, W., Siedlecki, M., 2013. Integral turbulence statistics over a Central European city Centre. Boundary-Layer Meteorol. 146, 257–276. doi:10.1007/s10546-012-9762-1

Grachev, A.A., Andreas, E.L., Fairall, C.W., Guest, P.S., Persson, P.O.G., 2015. Similarity theory based on the Dougherty-Ozmidov length scale. Q. J. R. Meteorol. Soc. 141, 1845–1856. doi:10.1002/qj.2488

Grachev, A.A., Andreas, E.L., Fairall, C.W., Guest, P.S., Persson, P.O.G., 2013. The critical Richardson number and limits of applicability of local similarity theory in the stable boundary layer. Boundary-Layer Meteorol. 147, 51–82. doi:10.1007/s10546-012-9771-0

Grachev, A.A., Andreas, E.L., Fairall, C.W., Guest, P.S., Persson, P.O.G., 2007. SHEBA flux-profile relationships in the stable atmospheric boundary layer. Boundary-Layer Meteorol. 124, 315–333. doi:10.1007/s10546-007-9177-6

Ha, K.-J., Hyun, Y.-K., Oh, H.-M., Kim, K.-E., Mahrt, L., 2007. Evaluation of boundary layer similarity theory for stable conditions in CASES-99. Mon. Weather Rev. 135, 3474–3483. doi:10.1175/MWR3488.1

Harman, I.N., Finnigan, J.J., 2010. Flow over hills covered by a plant canopy: Extension to generalised two-dimensional topography. Boundary-Layer Meteorol. 135, 51–65. doi:10.1007/s10546-009-9458-3

Hicks, B., 1978. Some limitations of dimensional analysis and power laws. Boundary-Layer Meteorol 14, 567–569. doi:10.1007/BF00121895

Högström, U., 1988. Non-dimensional wind and temperature profiles in the atmospheric surface layer: A re-evaluation. Boundary-Layer Meteorol. 42, 55–78. doi:10.1007/BF00119875

Högström, U., Bergström, H., Smedman, A.S., Halldin, S., Lindroth, A., 1989. Turbulent exchange above a pine forest, I: Fluxes and gradients. Boundary-Layer Meteorol. 49, 197–217. doi:10.1007/BF00116411

Holtslag, A.A.M., Nieuwstadt, F.T.M., 1986. Scaling the atmospheric boundary layer. Boundary-

Layer Meteorol. 36, 201–209. doi:10.1007/BF00117468
Howell, J., Mahrt, L., 1997. Multiresolution flux decomposition. Boundary-Layer Meteorol. 83, 117–137. doi:10.1023/A:1000210427798
Howell, J.F., Sun, J., 1999. Surface-layer fluxes in stable conditions. Boundary-Layer Meteorol. 90, 495–520. doi:10.1023/A:1001788515355
Kaimal, J.C., 1973. Turbulenece spectra, length scales and structure parameters in the stable surface layer. Boundary-Layer Meteorol. 4, 289–309. doi:10.1007/BF02265239
Kaimal, J.C., Finnigan, J.J., 1994. Atmospheric boundary layer flows: Their structure and measurement. University Press, New York.
Kaimal, J.C., Wyngaard, J.C., 1990. The Kansas and Minessota Experiments. Boudary-Layer Meteorlogy 50, 31–47.
Katul, G., Goltz, S.M., Hsieh, C.-I., Cheng, Y., Mowry, F., Sigmon, J., 1995. Estimation of surface heat and momentum fluxes using the flux-variance method above uniform and non-uniform terrain. Boundary-Layer Meteorol. 74, 237–260. doi:10.1007/BF00712120
Katul, G., Hsieh, C.I., Bowling, D., Clark, K., Shurpali, N., Turnipseed, A., Albertson, J., Tu, K., Hollinger, D., Evans, B., Offerle, B., Anderson, D., Ellsworth, D., Vogel, C., Oren, R., 1999. Spatial variability of turbulent fluxes in the roughness sublayer of an even-aged pine forest. Boundary-Layer Meteorol. 93, 1–28. doi:10.1023/A:1002079602069
Klipp, C.L., Mahrt, L., 2004. Flux-gradient relationship, self-correlation and intermittency in the stable boundary layer. Q. J. R. Meteorol. Soc. 130, 2087–2103. doi:10.1256/qj.03.161
Kljun, N., Calanca, P., Rotach, M.W., Schmid, H.P., 2015. A simple two-dimensional parameterisation for Flux Footprint Prediction (FFP). Geosci. Model Dev. 8, 3695–3713. doi:10.5194/gmd-8-3695-2015
Kral, S.T., Sjöblom, A., Nygård, T., 2014. Observations of summer turbulent surface fluxes in a High Arctic fjord. Q. J. R. Meteorol. Soc. 140, 666–675. doi:10.1002/qj.2167
Mahrt, L., 2014. Stably stratified atmospheric boundary layers. Annu. Rev. Fluid Mech. 46, 23–45. doi:10.1146/annurev-fluid-010313-141354
Mahrt, L., 2011. The near-calm stable boundary layer. Boundary-Layer Meteorol. 140, 343–360. doi:10.1007/s10546-011-9616-2
Mahrt, L., 2007. The influence of nonstationarity on the turbulent flux-gradient relationship for stable stratification. Boundary-Layer Meteorol 125, 245–264. doi:10.1007/s10546-007-9154-0
Mahrt, L., 2000. Surface heterogeneity and vertical structure of the boundary layer. Boundary-Layer Meteorol. 96, 33–62. doi:10.1023/A:1002482332477
Mahrt, L., Thomas, C., Richardson, S., Seaman, N., Stauffer, D., Zeeman, M., 2013. Non-stationary generation of weak turbulence for very stable and weak-wind conditions. Boundary-Layer Meteorol. 147, 179–199. doi:10.1007/s10546-012-9782-x
Mahrt, L., Vickers, D., Frederickson, P., Davidson, K., Smedman, A.-S., 2003. Sea-surface aerodynamic roughness. J. Geophys. Res. 108(C6), 3171. doi:10.1029/2002JC001383
Malhi, Y., 1996. The behaviour of the roughness length for temperature over heterogeneous surfaces. Q. J. R. Meteorol. Soc. 122, 1095–1125.
Marques Filho, E.P., Sá, L.D.A., Karam, H.A., Alvalá, R.C.S., Souza, A., Pereira, M.M.R., 2008. Atmospheric surface layer characteristics of turbulence above the Pantanal wetland regarding the similarity theory. Agric. For. Meteorol. 148, 883–892. doi:10.1016/j.agrformet.2007.12.004
Martins, C.A., Moraes, O.L.L., Acevedo, O.C., Degrazia, G.A., 2009. Turbulence intensity parameters over a very complex terrain. Boundary-Layer Meteorol. 133, 35–45. doi:10.1007/s10546-009-9413-3
Miller, N.E., Stoll, R., 2013. Surface heterogeneity effects on regional-scale fluxes in the stable boundary layer: Aerodynamic roughness length transitions. Boundary-Layer Meteorol. 149, 277–301. doi:10.1007/s10546-013-9839-5
Mironov, D. V, Sullivan, P.P., 2010. Effect of horizontal surface temperature heterogeneity on turbulent mixing in the stably stratified atmospheric boundary layer. 19th Amer. Meteorol.

Soc. Symp. Bound. Layers Turbul. CO, USA, 10 pp.
Mölder, M., Grelle, A., Lindroth, A., Halldin, S., 1999. Flux-profile relationships over a boreal forest - Roughness sublayer corrections. Agric. For. Meteorol. 98-99, 645–658. doi:10.1016/S0168-1923(99)00131-8
Monin, A.S., Obukhov, A.M., 1954. Basic laws of turbulent mixing in the surface layer of the atmosphere. Contrib. Geophys. Inst. Acad. Sci. USSR 24, 163–187.
Monteith, J.L., Unsworth, M.H., 1990. Principles of Environmental Physics, 2nd ed. Edward Arnold, London.
Moraes, O.L.L., Acevedo, O.C., Degrazia, G.A., Anfossi, D., da Silva, R., Anabor, V., 2005. Surface layer turbulence parameters over a complex terrain. Atmos. Environ. 39, 3103–3112. doi:10.1016/j.atmosenv.2005.01.046
Nadeau, D.F., Pardyjak, E.R., Higgins, C.W., Parlange, M.B., 2013. Similarity scaling over a steep alpine slope. Boundary-Layer Meteorol. 147, 401–419. doi:10.1007/s10546-012-9787-5
Nakamura, R., Mahrt, L., 2001. Similarity theory for local and spatially averaged momentum fluxes. Agric. For. Meteorol. 108, 265–279.
Nieuwstadt, F.T.M., 1984. The turbulent structure of the stable, nocturnal boundary layer. J. Atmos. Sci. doi:10.1175/1520-0469(1984)041<2202:TTSOTS>2.0.CO;2
Obukhov, A.M., 1946. Turbulence in an atmosphere with a non-uniform temperature. Boundary-Layer Meteorol. 2, 7–29.
Pahlow, M., Parlange, M.B., Porté-Agel, F., 2001. On Monin–Obukhov similarity in the stable atmospheric boundary layer. Boundary-Layer Meteorol. 99, 225–248.
Panofsky, H.A., Dutton, J.A., 1984. Atmospheric Turbulence: Models and Methods for Engineering Applications. John Wley and Sons, New York.
Rannik, Ü., 1998. On the surface layer similarity at a complex forest site. J. Geophys. Res. 103, 8685–8697.
Raupach, M.R., 1994. Simplified expressions for vegetation roughness length and zero-plane displacement as function of canopy height and area index. Boundary-Layer Meteorol. 71, 211–216.
Raupach, M.R., 1979. Anomalies in flux-gradient relationships over forest. Boundary-Layer Meteorol. 16, 467–486.
Raupach, M.R., Finnigan, J.J., Brunet, Y., 1996. Coherent eddies and turbulence in vegetation canopies: The mixing-layer analogy. Boundary-Layer Meteorol. 78, 351–382.
Rotach, M.W., 1993. Turbulence close to a rough urban surface. Part II: Variances and gradients. Boundary-Layer Meteorol. 66, 75–92.
Rotach, M.W., Andretta, M., Calanca, P., Weigel, A.P., Weiss, A., 2008. Boundary layer characteristics and turbulent exchange mechanisms in highly complex terrain. Acta Geophys. 56, 194–219. doi:10.2478/s11600-007-0043-1
Rotach, M.W., Calanca, P., 2014. Microclimate. Academic Press, pp. 258–264.
Rotach, M.W., Calanca, P., Graziani, P., Gurtz, J., Steyn, D.G., Vogt, R., Andretta, M., Christen, A., Cieslik, S., Connolly, R., De Wekker, S.F.J. and, Galmarini, S., Kadygrov, E.N., Kadygrov, V., Miller, E., Neininger, B., Rucker, M., van Gorsel, E., Weber, H., Weiss, A., Zappa, M., 2004. Turbulence structure and exchange processes in an Alpine Valley: The Riviera project. Bull. Am. Meteorol. Soc. 85, 1367–1385. doi:10.1175/BAMS-85-9-1367
Sanz Rodrigo, J., Anderson, P.S., 2013. Investigation of the stable atmospheric boundary layer at Halley Antarctica. Boudary-Layer Meteorlogy 148, 517–539. doi:10.1007/s10546-013-9831-0
Shaw, R.H., Finnigan, J.J., Patton, E.G., 2006. Eddy structure near the plant canopy interface. 17th Symp. Bound. Layers Turbul. J2.1.
Simpson, I.J., Thurtell, G.W., Neumann, H.H., Den Hartog, G., Edwards, G.C., 1998. The validity of similarity theory in the roughness sublayer above forests. Boundary-Layer Meteorol. 87, 69–99. doi:10.1023/A:1000809902980
Sorbjan, Z., Grachev, A.A., 2010. An evaluation of the flux – gradient relationship in the stable boundary layer. Boundary-Layer Meteorol. 135, 385–405. doi:10.1007/s10546-010-9482-3

Stiperski, I., Rotach, M.W., 2016. On the measurement of turbulence over complex mountainous terrain. Boundary-Layer Meteorol. 159, 97–121. doi:10.1007/s10546-015-0115-8

Stoll, R., Porté-Agel, F., 2008. Large-eddy simulation of the stable atmospheric boundary layer using dynamic models with different averaging schemes. Boundary-Layer Meteorol. 126, 1–28. doi:10.1007/s10546-007-9207-4

Stull, R.B., 1988. An Introduction to Boundary-Layer Meteorology. Kluwer Academic Publishers, Dordecht.

Thom, A.S., Stewart, J.B., Oliver, H.R., Gash, J.H.C., 1975. Comparison of aerodynamic and energy budget estimates of fluxes over a pine forest. Q. J. R. Meteorol. Soc. 101, 93–105. doi:10.1002/qj.49710142708

Trini Castelli, S., Falabino, S., 2013. Analysis of the parameterization for the wind-velocity fluctuation standard deviations in the surface layer in low-wind conditions. Meteorol. Atmos. Phys. 119, 91–107. doi:10.1007/s00703-012-0219-3

Večenaj, Ž., De Wekker, S.F.J., 2015. Determination of non-stationarity in the surface layer during the T-REX experiment. Q. J. R. Meteorol. Soc. 141, 1560–1571. doi:10.1002/qj.2458

Vickers, D., Mahrt, L., 2003. The cospectral gap and turbulent flux calculations. J. Atmos. Ocean. Technol. 20, 660–672. doi:10.1175/1520-0426(2003)20<660:TCGATF>2.0.CO;2

Wilczak, J., Oncley, S., Stage, S., 2001. Sonic anemometer tilt correction algorithms. Boundary-Layer Meteorol. 99, 127–150. doi:10.1023/A:1018966204465

Wood, C.R., Lacser, A., Barlow, J.F., Padhra, A., Belcher, S.E., Nemitz, E., Helfter, C., Famulari, D., Grimmond, C.S.B., 2010. Turbulent flow at 190 m height above London during 2006-2008: A climatology and the applicability of similarity theory. Boundary-Layer Meteorol. 137, 77–96. doi:10.1007/s10546-010-9516-x

Wyngaard, J.C., Coté, O.R., 1972. Cospectral similarity in the atmospheric surface layer. Q. J. R. Meteorol. Soc. 98, 590–603. doi:10.1002/qj.49709841708